
UNIVERSIDAD NACIONAL AUTÓNOMA DE MÉXICO
Posgrado en Astrofísica
INSTITUTO DE ASTRONOMÍA

# MULTICOLOR DIFFERENTIAL PHOTOMETRY OF CLOSE DOUBLE STARS

# T E S I S

QUE PARA OPTAR POR EL GRADO DE

MAESTRA EN CIENCIAS EN ASTROFÍSICA

P R E S E N T A:

Eunice Pérez Pérez

Tutores principales:

DR. VALERI ORLOV[1]
and
DR. LESTER IVAN FOX MACHADO[1]
[1]Instituto de Astronomía

Ciudad de México, Marzo, 2020

**Acknowledgments**

This research is supported by

DGAPA (Dirección General de Asuntos del Personal Académico) - UNAM
Programa de Apoyo a Proyectos de Investigación e Innovación Tecnológica (PAPIIT)

- PAPIIT IN107818: Fotometría rápida de enanas blancas pulsantes
  IP: PhD Valeri Orlov
- PAPIIT IN100918: Astrosismología y Binariedad: descifrando la estructura de estrellas en la Secuencia Principal
  IP: PhD Lester Ivan Fox Machado

## Summary

This project studies close binary stars with separations $\rho < 1''$ ; we present VRI differential photometric measurements of close double stars performed during April, 2019 with the 2.1m Telescope at the National Astronomical Observatory in the Sierra de San Pedro Mártir (SPM), Baja California, México. We report photometric and astrometric results for 114 resolved stars from the Washington Double Star Catalog (WDS) with angular separations ranging from $0''.2$ to $1''$ (very small separations) and magnitudes between 8 and 11. Using the Speckle Interferometry technique in three bands: Visible, Red and Infrared (Johnson-Cousin standard), we were able to calculate magnitude differences for 114 close double stars. After processing these data, we obtained results of the magnitude difference between the main and secondary components of the systems. Also, we obtained three correlation diagrams through the comparison of the magnitude differences between filters VRI, with dispersion of photometric measurements.

## Resumen

Este proyecto estudia estrellas binarias cercanas con separación $\rho < 1''$; se presentan mediciones de diferencias fotométricas VRI de estrellas binarias, observadas durante Abril, 2019 con el Telescopio de 2.1m en el Observatorio Astronómico Nacional en la Sierra de San Pedro Mártir (SPM), Baja California, México. Se reportan resultados fotométricos y astrométricos para 114 estrellas resueltas del catálogo Washington Double Star (WDS) con separación entre $0.''2$ y $1''$ (muy poco separadas) y de magnitud entre 8 y 11. Usando la técnica Speckle Interferometry (Interferometría de motas) en tres bandas: Visible, Rojo e Infrarrojo (Johnson-Cousin estándar), pudimos calcular diferencias de magnitud para 114 estrellas dobles cercanas. Después del procesamiento de estos datos, obtuvimos tres diagramas de correlación de la dispersión de los valores fotométricos.

# Contents

# 1

# Introduction

## 1.1 Importance of Photometry data

Classically, the observations of astronomical objects are made through their electromagnetic radiation, the study of the measurement of the flux or intensity radiated by celestial bodies is named photometry, from the Greek "photos" (light) and "meter" (measure). Photometry measures the visible light perceived by telescopes and special arrangements: spectrographs, interferometers and others. Photometry is used to estimate the physical characteristics of binary systems, such as the astrometry, the spectral type and the process of evolution; however, it is necessary to use a high-resolution technique to solve nearby binary systems $\rho \leq 1''$.

The method used to obtain the photometry of some object depends on the part of the electromagnetic spectrum studied, that is to say the observed wavelength. Basically, photometry is carried out by collecting electromagnetic radiation, passing it through optical bandpass filters, and then measuring light energy with a photosensitive instrument (CCD camera). The results of the observations are reported in standard bandpass sets (called photometric systems), defined to allow an accurate comparison of the observations.

Also, photometric data are used to construct the *Spectral Energy Distribution* (SED) of an object. Therefore, it is very important to collect as many photometric data as possible, in different regions of the spectrum, with different filters or photometric bands (Men'shchikov et al., 2006).

The photometric studies have many astronomical applications; as determine the luminosity of an object if its distance is known trough the combination of photometric measurements and the inverse square law. And other physical properties when using high

resolution spectroscopy, such as temperature, chemical composition and spectral class of the observed celestial object.

Photometry is also used to analyze the variability in the light intensity of objects such as stars in the stability range, active galactic nuclei, the evolution of supernovae (the total energy production during the explosion and the development of the expansion phase), to detect exoplanets in transit and determine their orbits. As for eclipsing binaries, it is possible to determine its period through the construction of a light curve (a graph of the light intensity of a celestial object, as a function of time) and calculate the radius of the system components.

Binary stars are found mainly in three different forms: visual binaries, photometric binaries and spectroscopic binaries; commonly, visual and photometric methods exclude the closest systems (closer than $1''$), because solving them requires a high-resolution technique. However, as we show below there are two methods to obtain differences of magnitude developed by Tokovinin & Cantarutti (2008) and Pluzhnik (2005), if the separation between components is higher than the seeing of the astronomical place of observation. In this thesis, we developed a method to measure difference in magnitudes between nearby components, in three filters: VRI.

The differences in magnitude between the filters constitute the color indices. To obtain the color index, the difference between filters B and V of the standard system is used. Another application of color indices is the *Color-Magnitude Diagram* (CMD), a graph of observational data from a set of stars that shows how the stellar population evolves in terms of its brightness (or luminosity) and color (surface temperature). The color of a star is interpreted as a measure of its surface temperature, because the stars can be considered as black body sources, which makes it possible to use Wien's Law and suggests a spectral type. The CMD is the observational version of the Hertzsprung-Russell diagram.

Although, it is known that double or multiple systems are more than 50% than individual stars (Karttunen, 2007), their study has been neglected to pursue other astrophysical objectives that appear to be more novel or promising. The large amount of data obtained by large surveys and satellites, boosted the development of galactic dynamics. However, they also provide many photometric measurements, useful for stellar study. A clear example was the complex reduction of the photometric signal for multiple objects, received from the satellite (Dommanget, 1993).

To describe the stellar evolution between components of multiple stars members of a cluster, is common to performer photometric observations in several filters and construct comparatives diagrams. In addition, the differential photometry of a nearby binary system

allows to obtain the internal temperature, the spectral classification of the components, the estimation of the effective temperature (color), to determine the evolutionary state of the components and the distribution of the mass.

The study of binary stars is the most useful direct way to connect stellar theoretical models with real observation parameters. For example, the *Mass-Luminosity Relation* (MLR) based on the masses of the components of the binary system. If the masses of the binary system, the photometry of both components and the distance are known, then it is possible to determine the absolute magnitude from the location of the system in a Mass-Luminosity diagram.

In the field of photometry, complementary data, such as color indices for double and multiple stars with at least two observed components, have proven to be very valuable for their astrophysical implications in the investigation of double stars. The most numerous photometric measurements of multi-star components were made by the HIPPARCOS (ESA, 1997) satellite, with narrow band filters. That makes comparison with our photometric results difficult, because we use photometric filters (broadband filters). However, the errors of the HIPPARCOS magnitude differences for close pairs that are weaker than 10m are often comparable with the measured values (Pluzhnik, 2005).

## 1.2 Observation of close double stars

The observation of double systems where the components distance is very small ($< 0.1''$), requires a high-resolution technique to be capable of resolving the atmospheres of each of the stars separately Each observation site has a characteristic seeing, which depends on its atmospheric turbulence; so that if the angle of separation between the components of the double system is smaller than the seeing, there is no direct method to obtain the photometry of each of the stars. However, with the technique speckle interferometry is possible to get the difference in magnitudes between them through analysis of the power spectrum PS of the system.

### 1.2.1 Double stars with close components

Binary systems are made up of two gravitationally attached nearby stars moving together through space. The three main types are described below:

- Optical doubles are stars which are not physically related to each other that appear to be together in the line of sight.
- Visual binaries are two stars gravitationally bound that can see visibly separated, with a basic instrument (telescope) or simple sight.

- Non-visual binaries are stars whose binary condition was concluded by external methods, such as occultation (eclipsing binaries), spectroscopy (spectroscopic binaries) or anomalies in their proper motions (astrometric binaries).

The *double optical stars* are due to the alignment of the line of sight between the position of the stars and the observer; they are usually very far from each other($> 5''$) and their proper motions (individual movements in right ascension and declination) are different. Unlike binary systems that are physically connected, gravitationally bound and orbit around a periodically common center of gravity, moving together in space.

In general, the position of the components of a double star are described by the separation and position angles. The separation angle is defined as the angular distance in arc seconds between the two components. Considering the brightest star (component A) as the origin, the position angle is measured from the dimmer star (component B) to the brightest in degrees, taking the north as 0° and east as 90°. It is common to represent these angles with Greek letters: the separation with rho ($\rho$) and position with theta ($\theta$). Another common term is $\Delta m$, which is the difference of magnitude measure between the primary and secondary stars (stars A and B respectively, as seen in Figure 1.1). The dimmer of the two stars is called a companion.

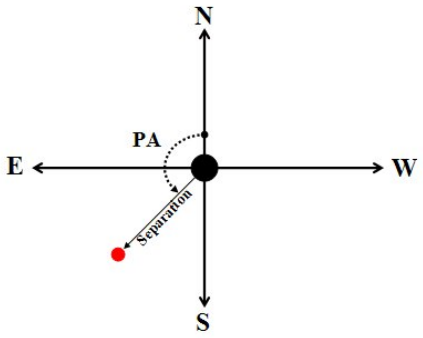


Figure 1.1: This figure shows a double system and its position angle (PA) $\theta$ and separation $\rho$.

The *visual binaries* are pairs of physically connected stars and can be seen as two separate components ($> 0.1''$). The relative position of the components changes as time goes on. A curve is the result of plotting the position and separation angles of several observations over years or decades. In the plot, if the orbital period is completed, the result is an ellipse. This ellipse is the apparent orbit, or the projection of the true orbit in the plane of the sky. The inclination of the orbital plane varies between 90° (with the observer in the line of sight) and 0° (the observer looking from above). Describing the

true orbit requires knowledge of the eccentricity of the ellipse, the inclination of the orbital plane and the orbital period in years (the time elapsed between successive arrivals of the star B to the periastron, that is, the moment when the two stars are closest).

The masses of the individual components can be determined by observing their relative movements, with respect to the center of mass. According to the definition of center of mass and with $a_1$ and $a_2$ the semi-major axes of the elliptical orbits of component A and B, respectively, the semi-major axes can be related to their masses as:

$$\frac{a_1}{a_2} = \frac{M_2}{M_1}, \tag{1.1}$$

where $M_1$ and $M_2$ are the masses of the components. That is to say, that the relative size of each orbit is inversely proportional to the mass of each star. In addition, the semi-major axis of the apparent orbit is given by $a = a_1 + a_2$. So, the total system mass is related to its orbit.

Using Kepler's Third Law and starting from the observations of the apparent orbit, one can determine the true orbit from the expression:

$$M_1 + M_2 = \frac{a^3}{\pi^3 P^2}, \tag{1.2}$$

where $a$ is the semi-major axis of the apparent ellipse, $\pi$ is the parallax (both given in arc seconds) and $P$ is the period (in years).

Using the equations 1.1 and 1.2 it is possible to obtain the mass of each component.

The *spectroscopic binaries* are stars that appear to be unique when seen from a telescope but observed through a spectroscope, their spectral lines change periodically over time due to the Doppler effect, with periods ranging from hours to a few decades. This Doppler effect is directly proportional to the radial velocity. Therefore, the separation of the spectral lines is greater when one component approaches the observer and the other moves away. Also, their period of variation is the orbital period of the system. To determine the actual velocity $v_0$, we start from the observed velocity $v$ from the expression:

$$v = v_0 sin(i), \tag{1.3}$$

where i is the angle of inclination between the line of sight and the normal to the orbital plane.

The *eclipsing binaries* have periodic variation in their total brightness due to the movement of the components of the system. That is, the periodic fading of light is caused

by the passage of one star in front of the other, because the orbital plane is almost in the line of sight of the observer. If the two stars are separated by a small distance and have almost the same size, there will be primary and secondary eclipses, depending on which component remains hidden. Eclipsing binaries tend to have periods of hours to days.

The *astrometric binaries* are seen as individual objects from a telescope, with the difference that they reveal their companion due to periodic changes in their proper motion. This movement is constant in a singular star, but the presence of a companion disturbs the movement of the main star and the effect is observed as a wobble. The first astrometric binary to be observed was Sirius in the 1830s, and due to its irregular proper motion, it was concluded that it has a companion, that star, Sirius B, was visually observed decades later and cataloged as a new object, distinctively, as a white dwarf.

More than half of the star systems in the universe have two or more members within them (Karttunen, 2007). Less common, but more spectacular are the *multiple stars* systems. In general, multiple systems have a hierarchical structure. For example, a star that orbits a binary system forms a triple system and two binary systems that orbit each other form a quadruple system. That is, multiple systems can be simply defined as several binary systems. Alpha Centauri, the closest star system to the Sun, is a triple star composed of two yellow dwarfs (Alpha Centauri A and Alpha Centauri B) and a red dwarf (Alpha Centauri C) that orbits around the other two.

### 1.2.2 History of the observation of double stars

The invention of the telescope in 1610 provided classical scientists with a revolutionary instrument for the observation of dark nights, which led to the discovery of several double systems; It was then that the Reverend John Michell first suggested that double stars were not only an effect of a coincidence in the line of sight, but as two components, moving around each other due to their mutual gravitational influence on one another, meaning that Newton's Laws were valid for objects outside the Solar System.

The first small double star catalog was compiled by Christian Mayer of Mannheim in 1780, but William Herschel, who improved the quality of his telescopes, also noted the existence of many more pairs of stars and developed a way to measure the stellar parallax. Herschel also discovered that the relative movement between two stars was curved and that could only be explained if the stars were orbiting around a common center of gravity. This is how the existence of binary stars was proven, even though, the mathematical confirmation came 6 years after his death. It was in 1828, that the French scientist Savary used $\xi$ Ursae Majoris (which Herschel had discovered) to show that the apparent orbit of the companion around the brightest star was elliptical. This work concluded on an

estimate of the ratio between stellar masses in a binary system. Which in the following 50 years caused a great desire by rich amateur astronomers in Europe, to observe double stars.

In 1857, an image of Mizar ($\zeta$ Ursae Majoris) with a 15 inches refractor telescope of Harvard was finally captured . However, the advantages of astro-photography for double star systems was not immediately perceived. This was because, the initial resolution did not allow the stellar systems with relatively short periods to be observed. On the other hand, the photography of bright systems with a big separation, such as 70 Ophiuchi, throughout its orbital cycle (19.7 days), made it possible to determine their individual masses from the apparent size of the ellipses traced by each of the components around the sky.

The speckle interferometry technique in 1970, was an important method used for the stellar reconstruction and study of binary stars. This technique efficiently eliminates the effects caused by the atmosphere and allows the telescope to function at the diffraction limit. The accuracy of this method is very good compared to other visual techniques. It has proven to be a valuable technique for the study of double systems with very little separation and long periods.

Then, the launch of the HIPPARCOS satellite in 1989, marked the beginning of a new era in the process of identifying double stars. Orbiting outside the atmosphere, the satellites slit detectors found $\sim$ 15000 new binary systems. A few years later, several special optical arrangements were built on the ground. Some of them are:

- In the UK, the five mirror interferometer COAST (Cambridge Optical Aperture Synthesis Telescope) operates with a baseline of 100 m (Baldwin et al., 1996).
- CHARA is an optical and IR interferometer of six elements in Mount Wilson in California; It has a range of baselines from 34 m to 330 m; it has four instruments working on the IR and two on visible (McAlister et al, 1990).
- The Very Large Telescope (VLT), located on the Cerro Paranal mountain in Chile consists of four telescopes with mirrors of 8.2m in diameter and another four with mirrors of 1.8m in diameter. Their telescopes can work individually or together as an interferometer that works like a telescope with mirror of 200 m in diameter (Lena, 1987).

Hence, the future of identifying and studying new binary systems is definitely in the development of new astronomical telescopes and space infrastructure. The successor of Hipparcos-Tycho, Gaia has already found millions of new double stars.

## 1.3 Arguments and critique

The papers previous to this thesis presented photometric results obtained mainly through two techniques: the first one was developed by Balega et al. (2002) and was applied by Pluzhnik (2005); it is based on analyzing the power spectrum until the cutoff frequency, with a ring method. The second by Tokovinin & Cantarutti (2008) proceeds by adjusting the power spectrum with the $P_0(f)$ model based on the spatial frequency and intensity. Both methods obtained few photometric measurements and mentioned the difficulty of comparing their measurements, made with photometric filters (broad filters), with the values of HIPPARCOS which uses narrow filters.

Taking advantage of previous results, we chose to use the method described in Section 1.3.2 of Pluzhnik (2005) but determining $C(\nu) = \frac{2\alpha_\nu}{\beta_\nu}$ by graphing $\alpha_\nu$ on the Y axis and $\beta_\nu$ on the X, and using a slope adjustment (as can be seen in Figure 2.8) and not by directly calculating the quotient between these variables; this avoids instabilities such as those shown in the final fits made by Pluzhnik (2005) (see Figure 1.5) and Balega et al. (2002) (see Figure 1.4). Also, this study is the first to present magnitude differences in the VRI system (Johnson & Cousins standard) and comparisons between filters.

## 1.4 Speckle interferometry observations of double systems

The speckle interferometry technique has been primarily used to determine binary star astrometry: angular separation and position angle. In general, speckle interferometry is a method that allows an angular resolution in the diffraction limit of the telescope to be obtained, when observing objects through a turbulent atmosphere.

Ideally, by using a circular aperture in a telescope without aberrations, a perfect image can be obtained. Meaning, an unresolved star with a radially symmetric point dispersion function (the distribution of two-dimensional intensity in the image of the star's energy, abbreviated PSF) along the optical axis, with a bright central core and a succession of concentric rings. This pattern is known as *Airy disk*.

Due to the circular symmetry of the Airy disk, it is possible to identify the center. When observing a binary star, there are two Airy disks, corresponding to the two sources not resolved of the system. As for astrometry, the angle of position and separation in unit of pixels are obtained from the image, therefore it is necessary to know the scale and orientation of the image to accurately calculate the astrometric parameters of the binary system.

The resolution lost by atmospheric turbulence can be recovered with interferometric

image reconstruction techniques, so it is important to mention that obtaining and processing images in the speckle interferometry technique are of great importance. To prevent the star disk from dominating the image, short exposures (20 ms or less) of the binary system are used, in the images obtained, speckles are shown that move randomly but confined in the central area. Each speckle is the power spectrum function of the star observed through the telescope.

### 1.4.1 The Airy Disk

In 1835 Airy described the structure of the image formed by passing light through a circular opening. The diffraction effect of a star produces concentric weak rings around a brighter center circle. The intensity of the Airy pattern is given by

$$I_{Airy}(r) = \left(\frac{2J_1(\alpha r)}{\alpha r}\right)^2, \tag{1.4}$$

where $r$ is the radial distance measured from the center, $J_1(\alpha r)$ are the Bessel functions of the first type of order one (of $\alpha r$), $\alpha = \frac{\phi D}{\lambda f}$, $D$ is the diameter of the aperture, $\lambda$ is the wavelength and $f$ is the focal length of the optical system.

To calculate the values of Bessel functions, numerical techniques are used. For now, it is only necessary to know the value at which $J_1(\alpha r)$ is zero, that is, when $\alpha r = 3.832$. So the diameter of the central peak of the Airy disc is given by:

$$\begin{aligned} D_{Airy} &= 2r \\ &= \frac{(2)(3.832)}{\alpha} \\ &= 2.44\frac{\lambda f}{D} \end{aligned} \tag{1.5}$$

The distribution of the brightness of a star on the Airy disk is such that, most of the light (84%) is located in the central disk, within the first dark ring. The intensity of the first bright ring is 7% of the total luminosity. The second bright ring represents only 3% and the remaining 6% is distributed on the outer rings.

### 1.4.2 Speckle Interferometry through the atmosphere

The atmosphere is the limiting factor for observations of objects in space from a high-resolution terrestrial optical telescope. The techniques used for the process of reconstruction of images obtained by speckle allow astronomers to overcome and efficiently eliminate atmospheric distortion and ensure that the performance of a terrestrial telescope is at the

limit of diffraction. Photon-noise, which limits the quality of image reconstruction, must be compensated by the calibration of the detector.

The resolution power of the telescope, or limit of detectable angular separation (i.e. between double stars), theoretically, is the smallest resolvable angle $\theta$ for a telescope with an objective lens or mirror of diameter $D$, for visible light ($\lambda \sim 560\ nm$), and it is given by:

$$\theta = \frac{0.12}{D} \tag{1.6}$$

where D is in meters and $\theta$ in arc seconds. If the atmosphere was not present, $\theta$ would be the resolution limit of the telescope.

However, atmospheric turbulence causes a point of light in space, such as a star, to be observed as a swollen or elongated image like a disk, when observed through terrestrial telescopes. Turbulence produces variations in the atmospheric density, temperature and refractive index. As an example of this is the visualization disk experiences a fast-apparent movement due to the instantaneous inclinations provoked by the wave fronts that reach the telescope. Moreover, from the scintillation of light that is visible to the naked eye, the signal of any detector in the focal plane of the telescope is affected. This blinking represents the changes in the fleeting brightness of a point source at frequencies of hundreds of Hz. Modifying the angular extent of the visual disk, causing a displacement of the image and causing scintillation as a consequence of the transition of the beam through the atmosphere.

Often, optimal observation sites are searched for, in order to improve the visibility of a telescope, places with a good environment with uniform temperature and free of any turbulent air (Beavers et al., 1989).

### 1.4.3 Basic model

F. Roddier proposed the basic model to describe the speckle interferometry technique as visual conditions due to atmospheric turbulence (Roddier, 1986). For which it is necessary to consider time intervals of less than 10 ms, so that atmospheric turbulence can be understood as a frozen pattern of phase variations.

The figure 1.2 shows an example of a frozen pattern for a short time. Where it is observed that the incoming wavefront of an object distant to the atmosphere is separated into constant phase cells of dimension $r_0$ in the plane of the telescope objective. In case there was no atmosphere, the incoming wavefront would have a constant phase over the entire surface of the target.

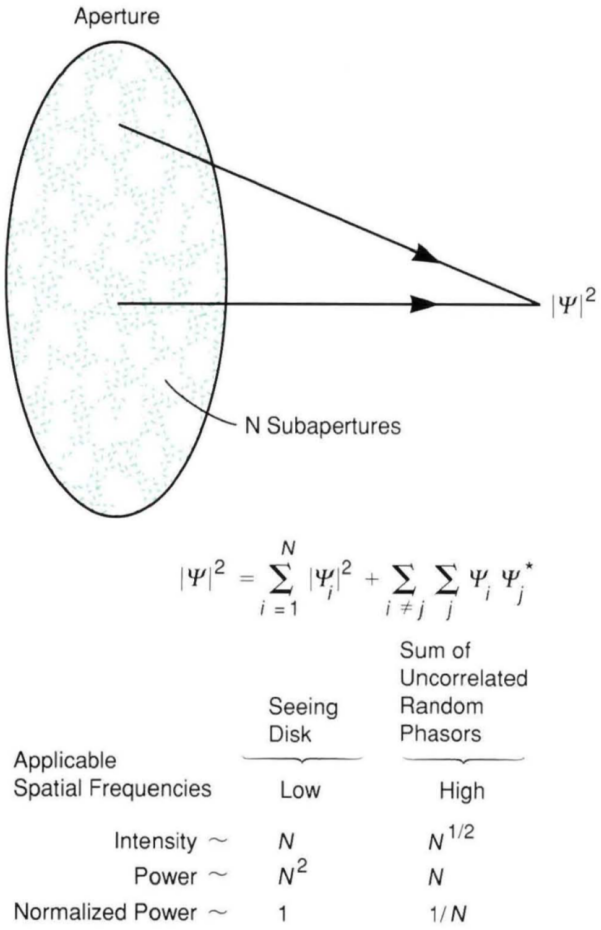


Figure 1.2: Division of telescope aperture into N effective sub-apertures. The image results from two independent terms with different N dependencies. The first term is given by the superposition of the intensities of the individual sub-openings, and the second term by the interference between the sub-openings. From Beavers et al. (1989).

At a later time interval, the new cell pattern is different in details but its statistical properties are similar (the size and number of constant phase cells or effective subapertures). Then, the sum of the contributions of all individual subapertures is used by diffraction theory to calculate the resulting image in the focal plane of the telescope. If we have $N$ subapertures with a complex amplitude $\Psi_i$, so that the complex amplitude $\Psi$ of the quasi-monochromatic field in the focal plane leads to an image intensity of

$$|\Psi|^2 = \left| \sum^{n=1} \Psi_i \right|^2 = \sum^{i=1} |\Psi_i|^2 + \sum_{i \neq j} \sum_{j} \Psi_i \Psi_j. \tag{1.7}$$

The instantaneous intensity of the image is the result of the sum of two different terms in the equation 1.7. The first term on the right side of the equation is the non-

coherent superposition of the intensities of the individual subapertures. Assuming that the subapertures are $r_0$, the diffraction limit $\theta_d$ for a subaperture is expressed as $\theta_d = \frac{0.12}{r_0}$. This contribution to image intensity does not contain high spatial frequency information. See figure 1.3 showing the relation between spatial frequencies in the focal plane and distances between the planes.

The second term is a sum of cross products, which describes the interference between the sub-openings, forming a multi-opening interferometer with random phase differences between the elements. Therefore, the second term contains high spatial frequency information of all combinations of orientation and baselines between subaperture pairs.

Then, the combination of the two terms in the equation 1.7 produces a snapshot of the vision disk, with two properties:

- The image fills the vision disk (described by the first term) within which there is a fine structure of bright spots, called motes (described by the second term).
- The points contain spatial frequency information up to the diffraction limit of the telescope and the point pattern changes rapidly (less than 10-20 ms).

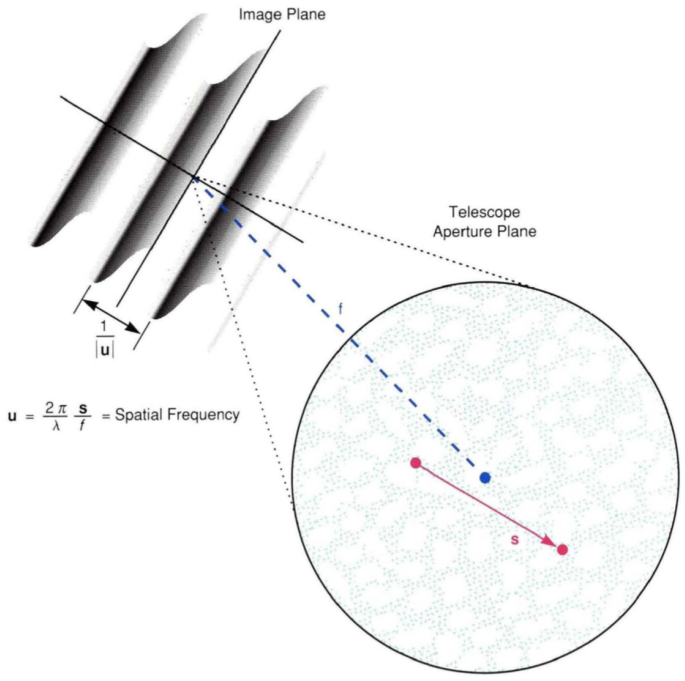


Figure 1.3: The relation between spatial frequencies in the image plane and the separations in the telescope aperture plane. From Beavers et al. (1989)

### 1.4.4 A solution to atmospheric distortion

Two approaches were taken to solve the problem of atmospheric distortion. The first approach uses a mirror that mechanically compresses the light path, correcting in real time the distortions of the wavefront. The second approach obtains a reconstructed image from the calculation of the Fourier transform of the combination of the amplitude and the phase map, product of the power spectrum of short exposures.

Labeyrie in 1970, developed a formalism (similar to the one presented below), with which it is possible to extract high spatial frequency information, through the speckle interferometry technique.

Let $i(x)$ be the two-dimensional image observed $i(x, y)$ and $o(x)$ the corresponding object of $o(x, y)$. The combined point-dispersion function of the telescope-atmosphere $t(x)$ describes the distribution of light when the telescope takes pictures of a source. Taking into consideration the isoplanatic case, whose fundamental premise of the mottled image, is that the short exposure image results from the convolution of the object and implicitly the function of scattering points is the same for all parts of the object. So, if the distortion is identical across the entire plane of the image, then the distortion is isoplanatic and is expressed as:

$$i(x) = o(x) * t(x), \tag{1.8}$$

where * denotes the two-dimensional convolution for the image process. In the Fourier transformation (spatial frequency representation) of the equation 1.8, the isoplanatic condition is expressed as

$$I(\nu) = O(\nu) \bullet T(\nu), \tag{1.9}$$

where $\nu$ is the two-dimensional spatial frequency variable corresponding to the spatial variable x.

Now, the power spectrum of the set of frames is described by the time average of the equation 1.9, given by:

$$\left\langle |I(\nu)|^2 \right\rangle = |O(\nu)|^2 \left\langle |T(\nu)|^2 \right\rangle . \tag{1.10}$$

The left side of the equation 1.10 is the power spectrum of the image, whose time average can be obtained from the collection of sequence of images with short exposures. The right side is the power spectrum of the object, which contains information about the amplitudes, and not about the phases of the object. For objects such as double stars, the

power spectrum reveals the angular separation, the orientation of the component (with an ambiguity of 180°) and the difference in magnitude between the stars. For more complex objects, the speckle interferometry technique is not appropriate.

## 1.5 Differential photometry solutions

### 1.5.1 Magnitude differences

Two methods used to obtain the difference in magnitude between components of a binary system are described below. Let A and B be the relative intents of these components, Balega et al. (2002) determined the marginal contrast $\frac{A^2+B^2}{AB}$ based on the spatial frequency for each concentric circle around the center of the average power spectrum up to the cutoff frequency at the diffraction limit (which quantifies the smallest object that an optical system can solve). The contrast of each of the circles depends on the $A/B$ flow ratio of the binary system and the photon bias (which depends on the shape of the event photon and can be obtained from the power spectrum).

The contrast of the stripes is dependent on the brightness of the binary system. That is, if the system is very bright, the photon bias is weak and has little influence on the contrast of stripes in the power spectrum, therefore it is independent of the radius of the circles and the intensity distribution; on the other hand, if the system is not very bright, the additive photon function depends on the radius of the power spectrum circles because the photon event is formed by extended points. The measurement of the contrast of bands depending on the radius is used to obtain the difference in magnitude between the components of the binary system, this method can be applied only if the power spectrum is formed by more than three bands (Figure 1.4).

### 1.5.2 Measurement of magnitude differences

A direct way of relating stellar theoretical models to observational parameters is the study of binary stars, for which the speckle interferometry technique is very useful, this is a method used mainly to obtain high-precision astrometry of multiple systems. Pluzhnik (2005) used this method to determine the difference in magnitude based on a standard power spectrum analysis of several series of speckles. Balega et al. (2002) and Balega et al. (2004) applied this technique in binary and multiple stars for observations made with the 6 m BTA telescope of the Special Astrophysical Observatory in Zelenchuk between 1998 and 1999

The method to determine the difference of magnitude $\Delta m$ through the interferometry is described below. First, are necessary measurements of the maximum amplitude ratio

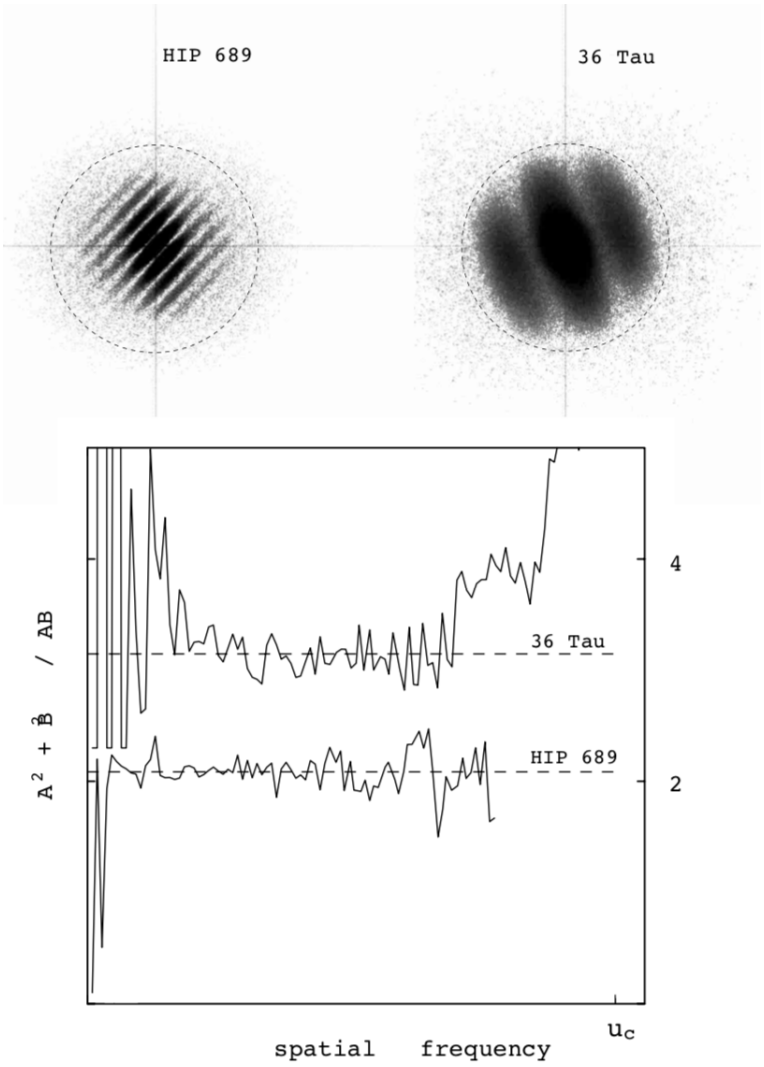


Figure 1.4: Above: Average power spectra of the set for HIP 689 and 36 Tau showing the stripes corresponding to the 0.″133 and 0.″032 separations. The dotted circles represent the diffraction cutoff frequency at 565 nm. Below: corresponding value of $\frac{A^2+B^2}{AB}$ depending on the spatial frequency. The cutoff limit $u_c$ is indicated. From Balega et al. (2002)

of the object for auto-correlation function or the contrast function between the power spectrum and the object visibility ratio. Since the noise is additive, the power spectrum of an interferometric pattern $\left\langle \left| I(\nu)^2 \right| \right\rangle$ can be expressed as

$$\left\langle \left| I(\nu)^2 \right| \right\rangle = |O(\nu)|^2 \left\langle \left| S(\nu)^2 \right| \right\rangle + N(\nu), \tag{1.11}$$

where $\nu$ is the spatial frequency vector, $O(\nu)$ is the Fourier transform of the intensity distribution of the object, $\left\langle \left| S(\nu)^2 \right| \right\rangle$ is the interferometric transfer function (STF) and $N(\nu)$ represents the power spectrum of noisy events.

Polarized photon noise and reading noise contribute additively to the function: $N(\nu) = N_p(\nu) + N_r(\nu)$. Modern detectors limit photon noise by reading, so the photon polarization term is much higher $N_p(\nu) >> N_r(\nu)$, because the reading noise term can be corrected easily. Therefore, only the influence of photon bias is considered.

Considering that $N_p(\nu) = N_0 n_p(\nu)$, where $n_p(\nu)$ is the normalized photon polarization term and $N_0$ is the photon polarization amplitude. The normalized photon bias $n_p(\nu)$ depends on the shape of the photon event and is determined through the normalized power spectrum of the flat field. The photon polarization amplitude is obtained from the analysis of the power spectrum beyond the cut-off frequency of the telescope (Airy disk), where $|O(\nu)|^2 \left\langle \left| S(\nu)^2 \right| \right\rangle = 0$. After correcting the photon bias, it is possible to deconvolve the equation 1.11 and obtain the astrometric parameters of the binary system, during the reconstruction of the system. This study is adequate to obtain positions, but calculating the difference in magnitude between components $\Delta m$ is still difficult to determine, due to the calibration of photon bias that affects the change in contrast between ranges of the power spectrum and the estimation of $\Delta m$. Therefore the following procedure is performed.

Assuming that the STF is circularly symmetric, it is possible to select an annular area for some spatial frequency $\nu$ small enough to consider $\left\langle \left| S(\nu)^2 \right| \right\rangle$ is constant. And if the value of the amplitude $N_0$ is fixed, then the astrometric parameters and photometric measurements in that annular area can be calculated using a least squares adjustment with a model function like the following:

$$F_2(\nu) = \alpha_\nu + \beta_\nu cos(2\pi\nu\rho), \tag{1.12}$$

where $\alpha_\nu$ and $\beta_\nu$ are unknown constants, and $\rho$ represents the unknown vector of separation. The mean values of the magnitude of the separation vector $\rho$ and the position angle $\theta$ are obtained for different annular areas and are used to determine $\Delta m$. The contrast function is defined as

$$C(\nu) = \frac{2\alpha_\nu}{\beta_\nu}. \tag{1.13}$$

So, for a binary system with components A and B, the contrast function $C(\nu)$ is

$$C(\nu) = \frac{A^2 + B^2}{AB} = \frac{A}{B} + \frac{B}{A}; \tag{1.14}$$

developing we have to

$$\begin{aligned} &\Rightarrow C(\nu)AB - (A^2 + B^2) = 0, \\ &\Rightarrow \frac{A^2 + B^2}{B^2} - \frac{C(\nu)AB}{B^2} = 0, \\ &\Rightarrow \left(\frac{A}{B}\right)^2 - C(\nu)\frac{A}{B} + 1 = 0. \end{aligned} \tag{1.15}$$

Let $x = \frac{A}{B}$, then we have

$$x^2 - C(\nu)x + 1 = 0, \tag{1.16}$$

whit positive solution:

$$x = \frac{C(\nu)}{2} + \sqrt{\left(\frac{C(\nu)}{2}\right)^2 - 1} = \frac{A}{B}, \tag{1.17}$$

The relation $x = \frac{A}{B}$ remains constant for all annular areas. However, if the value used for the amplitude $N_0$ is not the correct value, the contrast estimate increases towards higher frequencies. So, the correct value of the amplitude $N_0$ can be found under the condition $\frac{dC(\nu)}{d\nu} = 0 = C_1$. That it is fulfilled in a range of intermediate spatial frequencies; because at low frequencies the distortion effect of atmospheric seeing is strong, and at high frequencies the signal/noise ratio is low.

The value of $\frac{dC(\nu)}{d\nu}$ is determined from the first order slope adjustment

$$C(\nu) = C_0 + C_1\nu, \tag{1.18}$$

where $C_0$ (constant) and $C_1$ (pending) are unknown parameters.

Given the constant condition $C_1$ for which the amplitude $N_0$ was chosen, the intensity relation between the components $A/B$ is obtained from the equation:

$$\frac{A^2 + B^2}{AB} = \frac{A}{B} + \frac{B}{A} = C_0, \tag{1.19}$$

and therefore

$$\begin{aligned}\Delta m = m_A - m_B &= -2.5 \log \left( \frac{A}{B} \right) \\ &= -2.5 \log \left( \frac{C(\nu)}{2} + \sqrt{\left( \frac{C(\nu)}{2} \right)^2 - 1} \right)\end{aligned} \tag{1.20}$$

Figure 1.5 shows an example of the contrast function for binary systems HIP 114922 and HR 233, using the method described by Pluzhnik (2005).

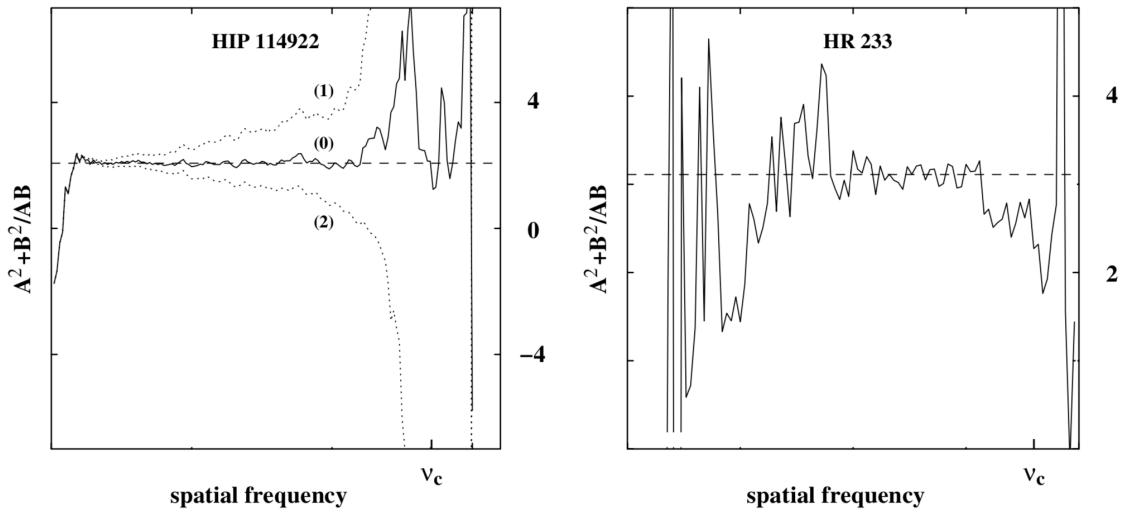


Figure 1.5: The contrast function as a function of spatial frequency for binary systems HIP 114922 ($\rho = 0.''107$, $V = 11.^m3$, $\Delta m = 0.^m16 \pm 0.^m09$, with photon polarization amplitudes $N_0^{(1)} = 0.93N_0^{(0)}$ and $N_0^{(2)} = 1.04N_0^{(0)}$) and HR 233 ($\rho = 0.''0160 \pm 0.''0005$, $V = 5.^m4$, $\Delta m = 1.^m08 \pm 0.^m\ 08$). $\nu_c$ is the cut-off limit of the telescope. From Pluzhnik (2005).

### 1.5.3 Relative photometry of binary components

A second method to obtain magnitude difference was developed by Tokovinin & Cantarutti (2008), who processed his data with the standard speckle method. First the photon bias is subtracted, and the power spectrum is accumulated and saved. The power spectrum $P(f)$ are normalized and $P(0) = 1$ are dominated by a strong peak at low frequencies (LF) and an extended halo high frequency (HF) corresponding to the speckle structure. The Figure 1.6 shows the power spectrum of a star $P_0(f)$ with noise subtraction. The (Dainty & Greenaway, 1979) theory predicts that $P_0(f)$ can be modeled as

$$P_0(f) \approx \exp[-3.44(f/f_c)^{\frac{5}{3}}(D/r_0)^{\frac{5}{3}}] + 0.435(D/r_0)^{-2}T_0(f), \tag{1.21}$$

where $f = |f|$ is the spatial frequency module, $D = 4.1m$ is the diameter of the telescope, $f_c = D/\lambda$ is the cutoff frequency, $r_0$ is the Fried parameter and $T_0(f)$ is the diffraction-limited transfer function, $T_0 = \frac{2}{\pi}\left[\arccos\left(\frac{f}{f_c}\right) - \left(\frac{f}{f_c}\right)\sqrt{1-\left(\frac{f}{f_c}\right)^2}\right]$ for $f < f_c$ and zero otherwise. The parameter $D/r_0$ is adjusted, it can be at the width of the LF part or at the level of $P_0(0.2f_c)$, similar values for both methods.

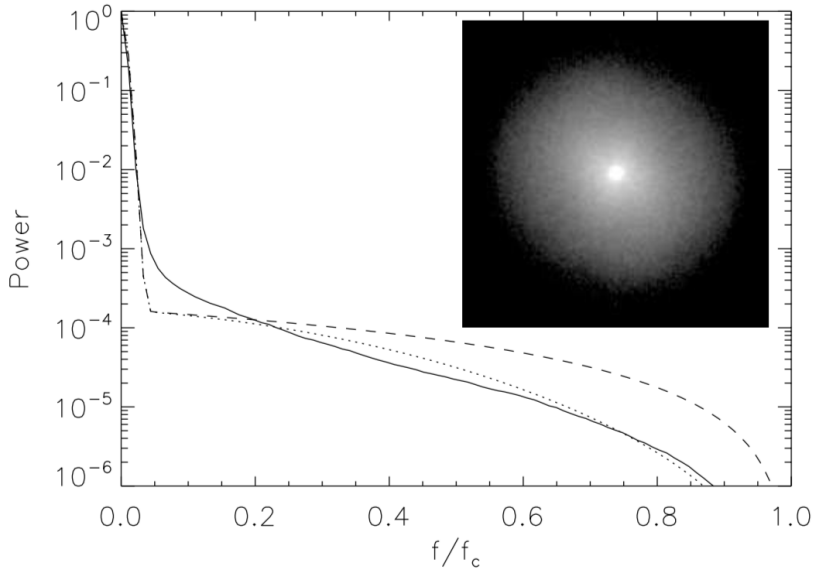


Figure 1.6: Power spectrum of star HR 1338, averaged radially and drawn as a complete line compared to the model with $D/r_0 = 50.8$ (dashed line). The dotted line is the same model with an additional Gaussian blur of 13 ms. The insert shows the two-dimensional spectrum on a logarithmic intensity scale in the range of $10 - 6to$ 10 -3. From Tokovinin & Cantarutti (2008).

To obtain the most important binary parameters (the separation $\rho$, the position angle $\theta$ and magnitude difference $\Delta m$) is necessary studying the power spectrum $P(f)$ as a fitted model, where the first two parameters are combined in a two-dimensional vector $r$ and $P_0(f)$ is the power spectrum of the single star reference. The model is given by:

$$P(f) = P_0(f)[A + B\cos(2\pi f r)] \tag{1.22}$$

The coefficients A and B define the relative scaling and magnitude difference. The contrast of power spectrum pattern or ratio of peaks in the auto correlation function (ACF) is expressed by the quotient $\beta = B/A = 2\alpha/(1+\alpha^2)$, then $\alpha = [1-(1-\beta^2)^{\frac{1}{2}}]/\beta$. If the intensity ratio $\alpha = 10^{-0.4\Delta m}$, hence the magnitude difference $\Delta m$ is

$$\Delta m = -2.5\log\left[\frac{1-(1-\beta^2)^{\frac{1}{2}}}{\beta}\right]. \tag{1.23}$$

For small $\Delta m$, the slope of this relation is minimal and this causes a greater error in relative photometry. In addition, if the contrast is underestimated, the value obtained from $\Delta m$ is also overestimated. Also the photon bias becomes significant for weak stars where the PS model fails.

# 2

# Observations and Data Reduction

At present, Observatorio Astronómico Nacional (OAN) has six telescopes working in the sierra de San Pedro Mártir (SPM) in Baja California, in the Northwest of México. One of them, is the 2.1 m telescope (see Figure 2.1) opened in 1979.

The OAN was constructed in the sierra SPM because the highest point of the observatory is located at 2830 m above sea level and the place where telescope is located is still a privileged place for astronomical observation: due to low light pollution, SPM has a very dark sky and a seeing about $1''$.

Figure 2.1: 2.1m telescope at El Observatorio Astronómico Nacional (OAN)

The speckle interferometry technique has been used at OAN since 2008 by Orlov et al. (2009) since this is the main method for accurate astrometric measurements. Speckle interferometry is also less expensive than other high resolution methods (such as adaptive optics) and provides a diffraction limited image in the visible range.

The data were obtained during one set of observations at the 2.1 meter telescope of OAN (see Figure 2.2). Speckle interferograms were taken during six nights in the spring of 2019, from April 19 to 24.

The observations were performed using the EMCCD iXon Ultra 888 from Andor Technology (Figure 2.3). This is a low-noise, high-sensitivity EMCCD camera. The camera can be cooled thermoelectrically down to $-95°$C which provides excellent elimination of read noise, even for the short time exposures. The detector has a quantum efficiency of more than 80% in the range of $450 - 750$nm, with maximum of 95% in the V-band (550nm).

This camera allows a fast frame rate so it can be used for high resolution imaging, in particular, speckle holography (Kohler, 2004). The detector has $1024 \times 1024$ square pixels of 13 $\mu m$ per side. We used a frame of $300 \times 300$ square pixels, because the size of a data cube for a binary system in three filters is around 1 GB.

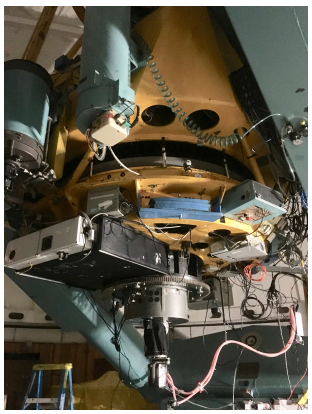

Figure 2.2: 2.1m telescope of the Observatorio Astronómico Nacional (OAN) with camera EMCCD iXon Ultra 888 from Andor Technology.

We used the $f/7.5$ secondary mirror combined with a microscope objective lens, with 5x amplifications and focal length approximately of 78.75m. After calibration, we determined a plate scale of 18.1 mas per pixel, given the telescope features mentioned above. As such parameters were not altered during the observation run, the plate scale remains the same for each night. The size of the diffraction-limited speckle ($d \approx \lambda$) for the 2.1m telescope is approximately 70 mas at the R filter wavelength. Given these parameters, we need an angular pixel scale of about 35 mas to obtain a Nyquist sample of these images, resulting in an angular pixel scale of 36.2 mas.

Although the use of broadband filters lowers the resolution, we aim to have results in a standard photometric system. Therefore, we used three *standard VRI filters* from the

Johnson-Cousins set. Typically, 1000 speckle frames of 300 × 300 pixel per object were taken with exposure times of $0.01737s$. We estimated that the seeing was better than $1''$ during all the observing nights. However, aberrations introduced by the telescope have a larger effect. Both astrometry and differential photometry results were obtained from the averaged power spectra by using the technique described in detail by Balega et al. (2002) and Pluzhnik (2005). The accuracy of this technique is excellent for measurements of component magnitude difference, separation, and position angle (the telescope has a resolution of $\rho \geq 0.''07$). The process includes Fourier analysis, correlation calculations of the second and third order, position measures of the components and relative photometry.


Figure 2.3: Camera EMCCD iXon Ultra 888 and filter wheel. Front and top view.

## 2.1 Processing

Each data cube is formed by one thousand frames or speckles, in three filters of Johnson and Cousins: V (Visible), R (Red) and I (Infrared), see Figure 2.5. The resolution of speckle interferometry for each filter is:

$\lambda_V/D = 0.''055$,
$\lambda_R/D = 0.''07$,
$\lambda_I/D = 0.''088$,

The first step of the data processing is the dark field correction of detected images $I'_n(\mathbf{x})$:

$$I_n(\mathbf{x}) = I'_n(\mathbf{x}) - Dark(\mathbf{x}), \tag{2.1}$$

where $\mathbf{x}$ is a 2D spatial coordinate, $I_n(\mathbf{x})$ is the corrected image, $Dark(\mathbf{x})$ is the averaged dark field (Figure 2.4 left).

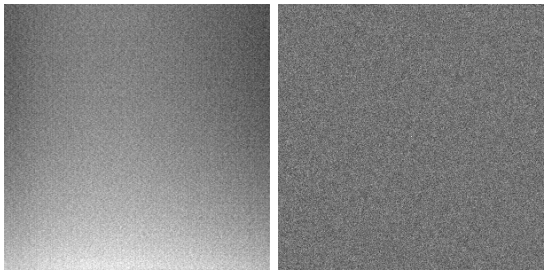

Figure 2.4: The averaged dark field $Dark(\mathbf{x})$ (left). The power spectrum of the photon event shape function $|G(\mathbf{f})|^2$ (right).

Below are shown as an example the speckles of the star 11258+5527 corrected by the dark field correction, with the three filters VRI.

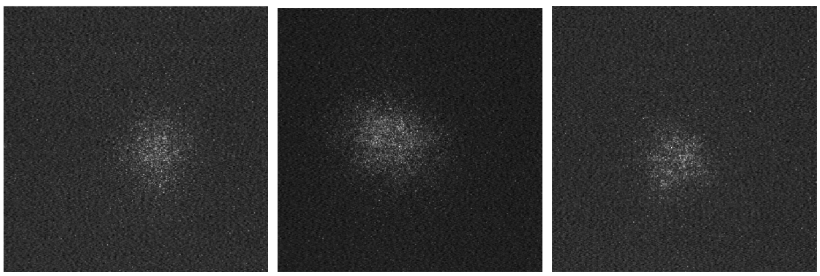

Figure 2.5: Example of speckles with three filters VRI (left to right) of star 11258+5527 observed on 21 April, 2019.

The next step is to calculate the averaged power spectrum (PS) for each star (Figure 2.6):

$$PS(\mathbf{f}) = \left\langle \left| FT\left\{ I_n(\mathbf{x}) \right\} \right|^2 \right\rangle, \tag{2.2}$$

where $\mathbf{f}$ is a spatial frequency, $FT\{...\}$ is the Fourier transform and $\langle ... \rangle$ denotes averaging over all images.

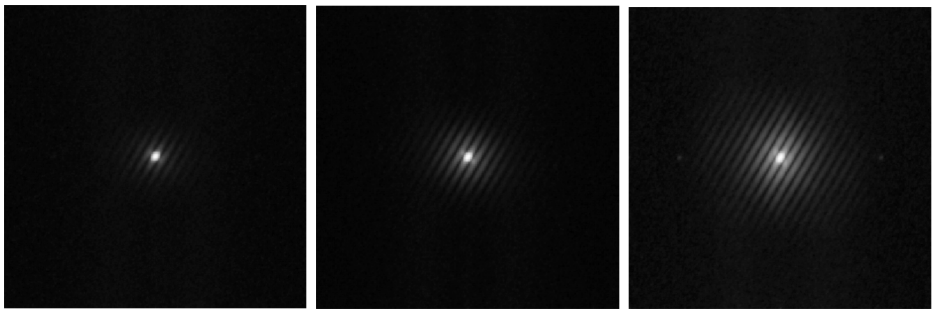

Figure 2.6: Example of the power spectrum with three filters VRI (left to right) of star 11258+5527 observed on 21 April, 2019.

In case of low light images, the averaged power spectrum can be expressed as (Kerp et al., 1992):

$$PS(\mathbf{f}) = P(\mathbf{f}) \cdot \left| G(\mathbf{f}) \right|^2 + q \left| G(\mathbf{f}) \right|^2, \tag{2.3}$$

where $P(\mathbf{f})$ is the unshifted estimation of the power spectrum, q is some constant, $\left|G(\mathbf{f})\right|^2$ is the power spectrum of the photon event shape function also known as photon bias. The photon bias $\left|G(\mathbf{f})\right|^2$ can be determined as the normalized power spectrum of the flat field frames. The good news is that the photon event shape function for iXon Ultra 888 is almost a delta function, so $\left|G(\mathbf{f})\right|^2$ is practically constant (Figure 2.4 right). Because the unshifted power spectrum of specklegrams is:

$$P(\mathbf{f}) = \left|O(\mathbf{f})\right|^2 \left\langle \left|S_n(\mathbf{f})\right|^2 \right\rangle, \tag{2.4}$$

the averaged power spectra can be expressed as:

$$PS(\mathbf{f}) = \left|O(\mathbf{f})\right|^2 \left\langle \left|S_n(\mathbf{f})\right|^2 \right\rangle + const, \tag{2.5}$$

where $\left|O(\mathbf{f})\right|^2$ power spectrum of the object, $\left\langle \left|S_n(\mathbf{f})\right|^2 \right\rangle$ is the speckle interferometric transfer function (STF).

In the case of double stars, the Equation 2.4 can be solved by least squares fitting with

a model function:

$$P_{mod}(\mathbf{f}) = P_0(\mathbf{f})\left[A + B\cos(2\pi\mathbf{fr})\right], \tag{2.6}$$

where $\mathbf{r} = (\rho\cos\theta, \rho\sin\theta)$ is a two-dimensional vector that determines the position of the component, and $B/A$ is the interferometric visibility $V$. The speckle transfer function (STF) $P_0(\mathbf{f})$ can be obtained by observing a reference star or by using an analytical model (Tokovinin & Cantarutti, 2008). However, one does not need to know the STF, in the case of circular symmetry (Pluzhnik, 2005). For any annular area with radius $\nu$ Eq. 2.5 can be solved by least squares fitting with a model function:

$$P_{mod}(\mathbf{f}_\nu) = \alpha_\nu + \beta_\nu\cos(2\pi\mathbf{f}_\nu\mathbf{r}) + const, \tag{2.7}$$

where $\alpha_\nu$ and $\beta_\nu$ are constants for the calculation of the interferometric visibility $V_\nu = \beta_\nu/\alpha_\nu$. We solve equation Eq. 2.7 for all frequencies with step=1 within the range $\nu_{min} < \nu < \nu_{max}$. Typically, we select $\nu_{min} = 0.1\nu_{cutoff}$ and $\nu_{max} = 0.9\nu_{cutoff}$, where $\nu_{cutoff}$ is the cutoff frequency of the telescope. Finally, we plot $\alpha_\nu$ as function of $\beta_\nu$.

As one can see, $\alpha_\nu$ and $\beta_\nu$ have a linear dependence and the visibility $V$ can be found by a least squares linear fitting of $\alpha_\nu = \beta_\nu/V + bias$ . When V is obtained, the magnitude difference $\Delta m$ is calculated by:

$$\Delta m = -2.5\log\left\{\frac{1-\sqrt{1-V^2}}{V}\right\}. \tag{2.8}$$

The brighter star is commonly taken as the primary, leaving the fainter one as the secondary component, though, this distinction depends on the used filter. In order to homogenize our results, we select as the primary component the brightest star of the system in the filter $V$. The power spectrum has a 180° ambiguity. To deal with this issue, we use the weighted shift-and-add analysis (Christou et al., 1986). The technique is self-calibrating for seeing effects, that is to say, it allows to get diffraction-limited images without using any reference star. When the components have a similar magnitude, the result of this technique is similar to the diffraction-limited autocorrelation; contrary to the case in which there is a clear difference between the components, as in Fig. 2.7. This technique is very sensitive to even small magnitude differences between the components, and it allows us overcome the common 180 degree ambiguity, thus obtaining a reconstruction of the close double star system. Then we can obtain the position angle and the separation angle.

Finally, the astrometry parameters are used to calculate magnitude differences, as described in Section 1.3.2 with the method developed by Pluzhnik (2005). But we do not

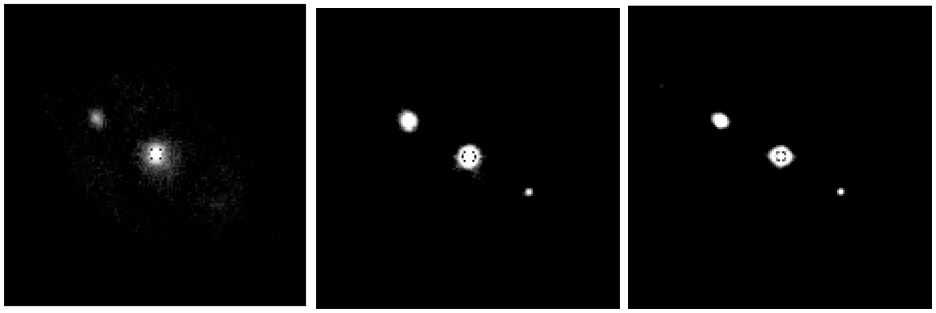

Figure 2.7: Example of the reconstruction of a system with three filters VRI (left to right) of star 11258+5527 (with average separation 1.″06) observed on 21 April, 2019.

directly fit the quotient $C(\nu) = \frac{2\alpha_\nu}{\beta_\nu}$. We find that it is more stable to graph $\alpha_\nu$ on the Y axis and $\beta_\nu$ on the X, and to use a slope fit by the method of least squares to obtain $C(\nu)$ value. Figure 2.8 shows an example for each filter.

1. Filter V:
   $\frac{\alpha_\nu}{\beta_\nu} = 1.5914$
   Photon Bias = 3.0001
   $\Delta(m) = 1.1292$

2. Filter R:
   $\frac{\alpha_\nu}{\beta_\nu} = 1.3652$
   Photon Bias = 0.8002
   $\Delta(m) = 0.9018$

3. Filter I:
   $\frac{\alpha_\nu}{\beta_\nu} = 1.2682$
   Photon Bias = 1.2754
   $\Delta(m) = 0.7785$

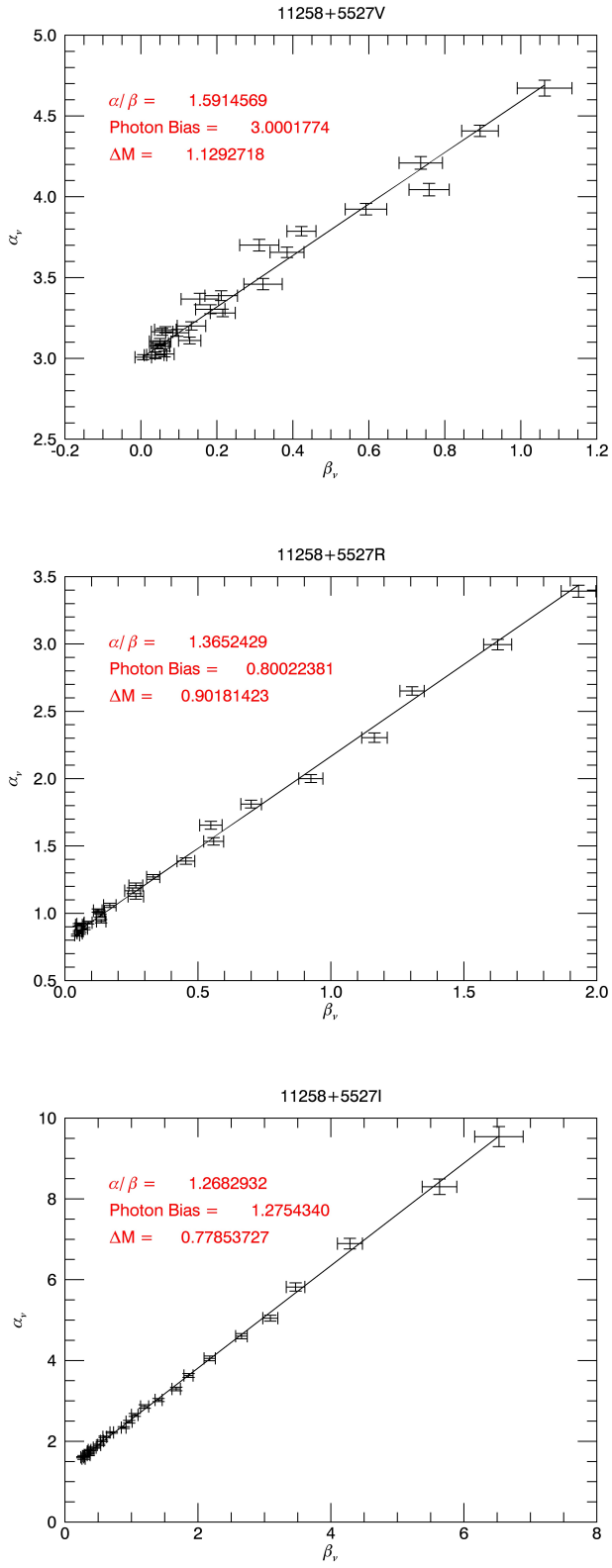


Figure 2.8: Example of slope fits using least squares to calculate $C(\nu)$, with three filters VRI (top to bottom) for star 11258+5527 observed on 21 April, 2019.

## 2.2 Calibration

For the astrometric calibration we selected 23 stars from our sample that fulfil the following criteria. The selection includes only the systems with more than one reliable observation from the INT4 catalogue (Fourth Catalog of Interferometric Measurements of Binary Stars) (Hartkopf et al., 2001). When the Hipparcos observations give several results for the same epoch of observation, we excluded those systems. We also excluded stars that were observed for the last time more than 20 years ago.

These 23 systems also have very slow movements and a large time base of observations; hence, we have been able to calculate the ephemerides of these stars for our epoch of observation using the linear approximation. A comparison with our data gives us the following offset for the position angle $\theta_0 = -3.61^\circ \pm 0.04^\circ$ and a scale in separation $s = 0''.03114 \pm 0''.00005$ per pixel. Comparing the corrected position angle and separation for our data with the reported values in the WDS, we found that the difference is about $0.7^\circ$ in position angle and $0''.003$ in separation.

Using the INT4 catalogue for our observation date, we calculated the ephemerides to corroborate this change minus the error; then we compared with the data of three different filters (resolved and with the weight center determined). We obtained that $\theta_{offset} = 0.''04$ and $\rho_{offset} = 5'' \times 10^{-5}$.

# 3

# Results

## 3.1 Differential Photometry Results

Table 3.1 presents our differential speckle photometric measurements. Column 1 give the designation of the double stars: the WDS catalog name Worley & Douglass (1997). Column 2 gives the epoch of observation in fractions of Besselian years (2019+). The following six columns contain the measured magnitude differences $\Delta m$ and their uncertainty $\sigma\Delta m$ for the three filters of the Johnson & Cousins system (VRI). And the last column gives the magnitude difference reported by the WDS catalog, between the magnitude 1 and magnitude 2; however, the filter used in that observations is not mentioned and therefore, is so difficult to do a rigorous comparison.

To present the magnitude differences is no necessary to use a standard system, however, we calculate the transformation coefficients for differential photometry as a example of this procedure (see Appendix). It is very important, to mention that we did not observe stars of reference; the magnitudes used for this fit were obtained from SIMBAD Astronomical Database; hence we did not check if this stars are variables. Also, our nights of observation had not the best photometric conditions, because we had faint clouds, full moon and other bad weather conditions.

Table 3.1: Differential photometry results of the April, 2019 observations.

| WDS (2000) | Epoch (2019+) | $\Delta$mI | $\sigma\Delta$mI | $\Delta$mR | $\sigma\Delta$mR | $\Delta$mV | $\sigma\Delta$mV | $m_1 - m_2$ |
|---|---|---|---|---|---|---|---|---|
| 20 April | | | | | | | | |
| 11151+3735 | 0.29955 | 1.390 | 0.019 | 0.756 | 0.035 | 0.871 | 0.030 | 0.88 |

Continued on the next page.

| WDS (2000) | Epoch (2019+) | ΔmI | σΔmI | ΔmR | σΔmR | ΔmV | σΔmV | $m_1 - m_2$ |
|---|---|---|---|---|---|---|---|---|
| 13062+1621 | 0.29972 | 1.012 | 0.029 | 1.103 | 0.027 | 1.168 | 0.034 | 0.20 |
| 13068+4022 | 0.29974 | 0.686 | 0.030 | 0.751 | 0.026 | 0.874 | 0.036 | 0.27 |
| 13134+5252 | 0.29980 | 0.505 | 0.029 | 0.526 | 0.038 | 0.773 | 0.041 | 0.03 |
| 13149+4055 | 0.29982 | 1.033 | 0.025 | 1.048 | 0.026 | 1.236 | 0.040 | 0.68 |
| 13225+4242 | 0.29986 | 1.254 | 0.012 | 1.192 | 0.019 | 1.166 | 0.024 | 0.78 |
| 13230+4058 | 0.29987 | 0.583 | 0.028 | 0.719 | 0.050 | 0.966 | 0.048 | 0.26 |
| 16013+4529 | 0.30010 | 1.160 | 0.014 | 1.389 | 0.020 | 1.454 | 0.025 | 0.03 |
| 16028+4902 | 0.30012 | 0.553 | 0.022 | 0.455 | 0.034 | 0.864 | 0.057 | 0.18 |
| 16043+3230 | 0.30014 | 2.687 | 0.008 | 2.616 | 0.011 | 2.508 | 0.014 | 2.46 |
| 21 April | | | | | | | | |
| 11247+3758 | 0.30221 | 1.157 | 0.016 | 1.152 | 0.018 | 1.505 | 0.021 | 0.28 |
| 11258+5527 | 0.30223 | 0.781 | 0.019 | 0.902 | 0.018 | 1.129 | 0.027 | 0.75 |
| 11287+3224 | 0.30226 | 0.229 | 0.070 | 0.203 | 0.063 | 0.430 | 0.048 | 0.31 |
| 11297+3302 | 0.30228 | 0.317 | 0.057 | 0.250 | 0.066 | 0.293 | 0.055 | 0.32 |
| 11336+4729 | 0.30229 | 0.245 | 0.064 | 0.258 | 0.056 | 0.219 | 0.082 | 0.28 |
| 11397+5036 | 0.30231 | 1.045 | 0.027 | 0.960 | 0.025 | 1.162 | 0.048 | 0.50 |
| 11431+3715 | 0.30233 | 0.745 | 0.023 | 0.772 | 0.028 | 0.809 | 0.022 | 0.16 |
| 11463+3131 | 0.30234 | 0.350 | 0.071 | 0.220 | 0.085 | 0.227 | 0.120 | 0.00 |
| 11487+3937 | 0.30235 | 0.945 | 0.023 | 0.919 | 0.021 | 1.098 | 0.022 | 0.17 |
| 11487+4030 | 0.30234 | 0.487 | 0.040 | 0.441 | 0.039 | 0.506 | 0.034 | 0.21 |
| 11499+3754 | 0.30236 | 0.269 | 0.051 | 0.326 | 0.054 | 0.464 | 0.043 | 0.21 |
| 15034+3342 | 0.30264 | 0.745 | 0.030 | 0.891 | 0.026 | 0.807 | 0.020 | 0.36 |
| 15062+5225 | 0.30270 | 0.810 | 0.028 | 0.884 | 0.028 | 1.023 | 0.036 | 0.17 |
| 15075+5516 | 0.30270 | 0.167 | 0.080 | 0.160 | 0.069 | 0.359 | 0.049 | 0.30 |
| 15088+4014 | 0.30271 | 0.000 | 0.186 | 0.000 | 0.185 | 0.000 | 0.214 | 0.00 |
| 15136+3453 | 0.30275 | 0.119 | 0.063 | 0.255 | 0.037 | 0.316 | 0.027 | 0.10 |
| 15154+3558 | 0.30276 | 0.282 | 0.041 | 0.305 | 0.031 | 0.328 | 0.040 | 0.50 |
| 15192+4329 | 0.30283 | 0.577 | 0.032 | 0.614 | 0.038 | 0.746 | 0.039 | 0.50 |
| 15200+4603 | 0.30284 | 0.593 | 0.034 | 0.605 | 0.044 | 0.660 | 0.072 | 0.28 |
| 22 April | | | | | | | | |
| 18062+3326 | 0.30537 | 0.679 | 0.033 | 0.747 | 0.035 | 0.641 | 0.048 | 0.00 |
| 14040+4314 | 0.30487 | 1.152 | 0.024 | 1.239 | 0.018 | 1.451 | 0.021 | 0.02 |
| 14048+3243 | 0.30487 | 0.410 | 0.052 | 0.471 | 0.044 | 0.630 | 0.048 | 0.02 |
| 14059+3848 | 0.30489 | 0.308 | 0.057 | 0.363 | 0.052 | 0.459 | 0.071 | 0.00 |
| 14059+4059 | 0.30489 | 0.421 | 0.055 | 0.426 | 0.052 | 0.532 | 0.058 | 0.25 |

Continued on the next page.

| WDS (2000) | Epoch (2019+) | ΔmI | σΔmI | ΔmR | σΔmR | ΔmV | σΔmV | $m_1 - m_2$ |
|---|---|---|---|---|---|---|---|---|
| 14122+4411 | 0.30492 | 0.307 | 0.035 | 0.381 | 0.028 | 0.338 | 0.034 | 0.33 |
| 14171+4529 | 0.30496 | 0.536 | 0.024 | 0.620 | 0.021 | 0.684 | 0.026 | 0.60 |
| 14171+5100 | 0.30497 | 0.763 | 0.018 | 0.929 | 0.018 | 1.073 | 0.022 | 1.30 |
| 14184+3412 | 0.30499 | 1.130 | 0.017 | 1.216 | 0.018 | 1.305 | 0.017 | 0.08 |
| 14188+5934 | 0.30499 | 1.293 | 0.014 | 1.290 | 0.030 | 1.395 | 0.041 | 0.12 |
| 14220+5107 | 0.30503 | 0.262 | 0.057 | 0.389 | 0.056 | 0.401 | 0.068 | 0.64 |
| 14289+4226 | 0.30529 | 0.536 | 0.038 | 0.633 | 0.038 | 0.783 | 0.058 | 0.32 |
| 18017+4011 | 0.30531 | 0.173 | 0.075 | 0.262 | 0.042 | 0.148 | 0.073 | 0.43 |
| 18036+3731 | 0.30531 | 0.882 | 0.021 | 1.044 | 0.016 | 1.413 | 0.019 | 0.34 |
| 18054+4306 | 0.30534 | 0.619 | 0.058 | 0.875 | 0.025 | 0.837 | 0.030 | 0.15 |
| 18054+5155 | 0.30535 | 0.892 | 0.024 | 0.872 | 0.025 | 0.957 | 0.033 | 0.39 |
| 18063+3824 | 0.30538 | 0.000 | 0.136 | 0.000 | 0.136 | 0.000 | 0.159 | 0.22 |
| 18064+4437 | 0.30539 | 0.353 | 0.092 | 0.293 | 0.108 | 0.361 | 0.138 | 0.00 |
| 10056+3105 | 0.30546 | 0.814 | 0.023 | 0.933 | 0.021 | 1.023 | 0.015 | 1.05 |
| 10059+5731 | 0.30548 | 1.154 | 0.017 | 1.065 | 0.036 | 1.076 | 0.035 | 0.20 |
| 10095+4126 | 0.30568 | 0.474 | 0.036 | 0.512 | 0.030 | 0.565 | 0.029 | 0.12 |
| 10118+4222 | 0.30570 | 0.722 | 0.043 | 0.736 | 0.040 | 0.830 | 0.040 | 0.06 |
| 10164+4003 | 0.30572 | 0.774 | 0.033 | 0.841 | 0.035 | 1.123 | 0.029 | 0.19 |
| 10261+5347 | 0.30576 | 0.472 | 0.056 | 0.537 | 0.072 | 0.584 | 0.064 | 0.09 |
| 23 April | | | | | | | | |
| 12056+5659 | 0.30773 | 0.086 | 0.081 | 0.218 | 0.097 | 0.199 | 0.124 | 0.80 |
| 12080+4242 | 0.30786 | 0.505 | 0.025 | 0.501 | 0.028 | 0.347 | 0.064 | 0.49 |
| 12092+5013 | 0.30788 | 0.620 | 0.044 | 0.774 | 0.058 | 0.000 | 0.421 | 0.46 |
| 12160+4807 | 0.30792 | 0.365 | 0.053 | 0.448 | 0.049 | 0.441 | 0.066 | 0.42 |
| 12195+4456 | 0.30792 | 0.604 | 0.041 | 0.718 | 0.040 | 0.707 | 0.098 | 0.61 |
| 12215+5014 | 0.30794 | 0.312 | 0.094 | 0.000 | 0.236 | 0.000 | 0.324 | 0.10 |
| 16026+4658 | 0.30813 | 0.866 | 0.028 | 0.790 | 0.020 | 0.869 | 0.037 | 0.92 |
| 16028+4902 | 0.30815 | 0.192 | 0.046 | 0.213 | 0.047 | 0.310 | 0.083 | 0.18 |
| 16061+5652 | 0.30821 | 0.860 | 0.016 | 1.033 | 0.023 | 1.482 | 0.028 | 0.34 |
| 16097+4900 | 0.30824 | 0.415 | 0.036 | 0.397 | 0.034 | 0.331 | 0.068 | 0.24 |
| 16107+4019 | 0.30825 | 0.923 | 0.015 | 0.948 | 0.015 | 1.034 | 0.016 | 0.53 |
| 16128+3922 | 0.30827 | 0.484 | 0.024 | 0.543 | 0.024 | 0.576 | 0.025 | 0.74 |
| 16137+4638 | 0.30828 | 0.984 | 0.012 | 1.143 | 0.012 | 1.123 | 0.021 | 0.52 |
| 16140+4200 | 0.30828 | 0.466 | 0.028 | 0.342 | 0.030 | 0.332 | 0.069 | 0.00 |
| 16172+3341 | 0.30829 | 0.254 | 0.061 | 0.206 | 0.063 | 0.000 | 0.244 | 0.36 |

Continued on the next page.

| WDS (2000) | Epoch (2019+) | ΔmI | $\sigma$ΔmI | ΔmR | $\sigma$ΔmR | ΔmV | $\sigma$ΔmV | $m_1 - m_2$ |
|---|---|---|---|---|---|---|---|---|
| 16173+5001 | 0.30830 | 0.330 | 0.040 | 0.311 | 0.054 | 0.412 | 0.058 | 0.03 |
| 16178+4918 | 0.30831 | 0.299 | 0.044 | 0.404 | 0.047 | 0.474 | 0.038 | 0.14 |
| 16192+4140 | 0.30832 | 0.195 | 0.041 | 0.000 | 0.144 | 0.000 | 0.145 | 0.23 |
| 16216+3631 | 0.30833 | 0.000 | 0.151 | 0.186 | 0.058 | 0.231 | 0.057 | 0.00 |
| 24 April | | | | | | | | |
| 10477+2733 | 0.31051 | 0.329 | 0.058 | 0.295 | 0.087 | 0.318 | 0.094 | 0.30 |
| 10486+3532 | 0.31050 | 0.671 | 0.037 | 0.653 | 0.041 | 0.713 | 0.048 | 0.30 |
| 10529+2209 | 0.31042 | 0.630 | 0.024 | 0.644 | 0.021 | 0.596 | 0.032 | 0.19 |
| 10543+2607 | 0.31041 | 0.299 | 0.061 | 0.431 | 0.028 | 0.441 | 0.030 | 0.09 |
| 10544+2044 | 0.31039 | 0.881 | 0.020 | 0.928 | 0.011 | 1.002 | 0.013 | 0.06 |
| 10544+3840 | 0.31036 | 0.000 | 0.171 | 0.000 | 0.156 | 0.000 | 0.168 | 0.21 |
| 10548+2345 | 0.31035 | 0.736 | 0.022 | 1.033 | 0.010 | 1.371 | 0.008 | 0.93 |
| 10567+3320 | 0.31030 | 0.244 | 0.063 | 0.270 | 0.042 | 0.217 | 0.040 | 0.04 |
| 10574+0147 | 0.31034 | 0.596 | 0.038 | 0.522 | 0.068 | 0.346 | 0.157 | 0.01 |
| 10585+1711 | 0.31032 | 0.000 | 0.169 | 0.110 | 0.080 | 0.000 | 0.183 | 0.41 |
| 14317+3554 | 0.30817 | 0.479 | 0.072 | 0.458 | 0.062 | 0.391 | 0.136 | 0.53 |
| 14340+4500 | 0.31090 | 0.262 | 0.078 | 0.120 | 0.147 | 0.175 | 0.146 | 0.24 |
| 14460+4723 | 0.31082 | 0.311 | 0.046 | 0.291 | 0.053 | 0.555 | 0.040 | 0.42 |
| 14487+4513 | 0.31081 | 0.503 | 0.051 | 0.539 | 0.037 | 0.320 | 0.107 | 0.88 |
| 14492+4814 | 0.31081 | 0.000 | 0.158 | 0.342 | 0.034 | 0.504 | 0.026 | 0.30 |
| 14515+4456 | 0.31080 | 0.094 | 0.110 | 0.244 | 0.044 | 0.318 | 0.040 | 0.22 |
| 14558+3939 | 0.31078 | 0.384 | 0.027 | 0.377 | 0.022 | 0.409 | 0.018 | 0.00 |
| 14571+5136 | 0.31077 | 0.348 | 0.059 | 0.313 | 0.056 | 0.000 | 0.314 | 0.03 |
| 14575+3124 | 0.31076 | 0.125 | 0.102 | 0.327 | 0.057 | 0.000 | 0.470 | 0.18 |
| 14593+4649 | 0.31074 | 0.773 | 0.013 | 1.040 | 0.011 | 1.287 | 0.012 | 0.86 |
| 16013+4529 | 0.31094 | 1.032 | 0.020 | 1.032 | 0.018 | 1.124 | 0.019 | 0.03 |
| 16026+4658 | 0.31097 | 0.677 | 0.035 | 0.733 | 0.026 | 0.695 | 0.036 | 0.92 |
| 16028+4902 | 0.31096 | 0.086 | 0.102 | 0.000 | 0.156 | 0.000 | 0.261 | 0.18 |
| 16107+4019 | 0.31104 | 0.923 | 0.033 | 0.939 | 0.030 | 1.065 | 0.027 | 0.53 |
| 16118+3424 | 0.31104 | 1.126 | 0.012 | 0.847 | 0.016 | 0.674 | 0.015 | 0.52 |
| 25 April | | | | | | | | |
| 09043+4008 | 0.31303 | 0.780 | 0.026 | 0.787 | 0.027 | 0.870 | 0.026 | 0.72 |
| 09067+5038 | 0.31305 | 0.000 | 0.174 | 0.000 | 0.228 | 0.000 | 0.238 | 0.06 |
| 09100+4034 | 0.31307 | 0.000 | 0.198 | 0.000 | 0.229 | 0.000 | 0.245 | 0.28 |
| 09171+4040 | 0.31310 | 1.047 | 0.021 | 1.127 | 0.025 | 1.055 | 0.027 | 0.29 |

Continued on the next page.

| WDS (2000) | Epoch (2019+) | ΔmI | $\sigma$ΔmI | ΔmR | $\sigma$ΔmR | ΔmV | $\sigma$ΔmV | $m_1 - m_2$ |
|---|---|---|---|---|---|---|---|---|
| 09172+4038 | 0.31311 | 0.733 | 0.032 | 0.805 | 0.033 | 0.808 | 0.034 | 0.70 |
| 09224+4616 | 0.31313 | 0.235 | 0.068 | 0.000 | 0.248 | 0.000 | 0.274 | 0.00 |
| 13033+3435 | 0.31340 | 0.192 | 0.072 | 0.327 | 0.034 | 0.397 | 0.034 | 0.00 |
| 13068+4022 | 0.31345 | 0.191 | 0.087 | 0.222 | 0.052 | 0.211 | 0.070 | 0.27 |
| 13120+4703 | 0.31347 | 0.000 | 0.162 | 0.139 | 0.087 | 0.217 | 0.062 | 0.00 |
| 13134+5252 | 0.31349 | 0.088 | 0.103 | 0.000 | 0.236 | 0.000 | 0.255 | 0.03 |
| 13149+4055 | 0.31350 | 0.819 | 0.024 | 0.836 | 0.023 | 0.947 | 0.027 | 0.68 |
| 17007+3951 | 0.31374 | 0.136 | 0.103 | 0.000 | 0.165 | 0.000 | 0.158 | 0.11 |
| 17043+4445 | 0.31378 | 0.967 | 0.019 | 1.080 | 0.012 | 1.133 | 0.011 | 0.14 |
| 17073+4604 | 0.31379 | 0.538 | 0.041 | 0.421 | 0.034 | 0.504 | 0.026 | 0.29 |
| 17075+5126 | 0.31381 | 0.581 | 0.042 | 0.473 | 0.040 | 0.525 | 0.046 | 0.30 |
| 17076+4108 | 0.31382 | 1.564 | 0.020 | 1.503 | 0.020 | 1.605 | 0.018 | 2.00 |
| 17088+4856 | 0.31383 | 0.143 | 0.094 | 0.230 | 0.069 | 0.341 | 0.057 | 0.30 |

### 3.1.1 Diagrams

The magnitude difference for the red filter is larger than that for the blue one (this is something to be expected given that, in general, the secondary stars are of late type), as we can see by the value of the slope in equations 3.1 and 3.2. In the scatter diagrams (Figures 3.1, 3.2 y 3.3) there is a correlation between the magnitude differences measured with the different filters. The results show clearly the linear correlation between any pair of filters. We present the numerical estimates of those correlations and their errors:

$$\Delta mI = (0.9466 \pm 0.02779)\Delta mR + (0.0065 \pm 0.0200) \tag{3.1}$$

$$\Delta mI = (0.7959 \pm 0.1393)\Delta mV + (0.0558 \pm 0.1099) \tag{3.2}$$

$$\Delta mR = (0.8457 \pm 0.1450)\Delta mV + (0.0490 \pm 0.1144) \tag{3.3}$$

This is a preliminary estimation, obtained using only 114 stars. Once we have processed more data (a new observational set of August, 2019), we will provide a more detailed analysis.

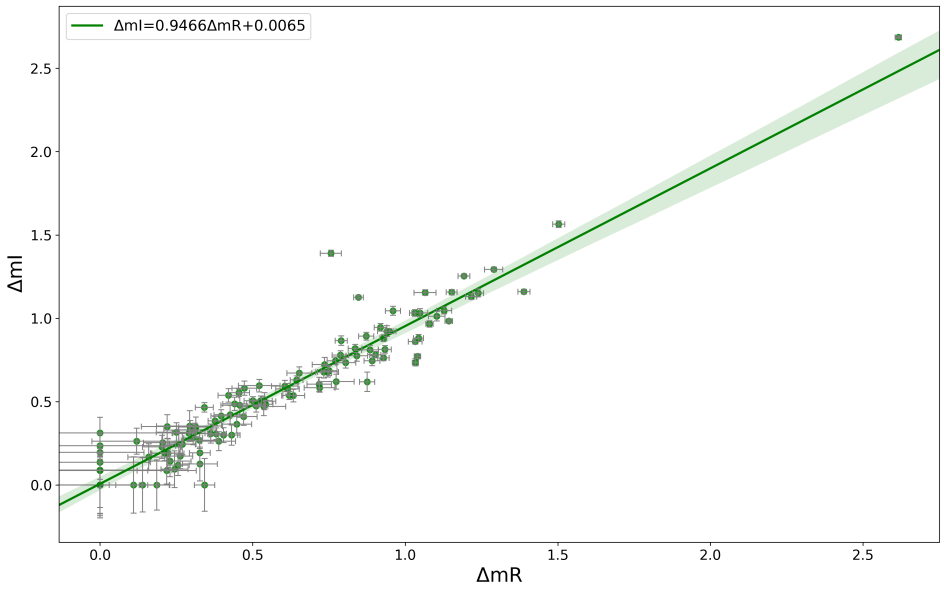


Figure 3.1: Correlation of the magnitude difference between filters Infrared and Red. $R = 0.955$

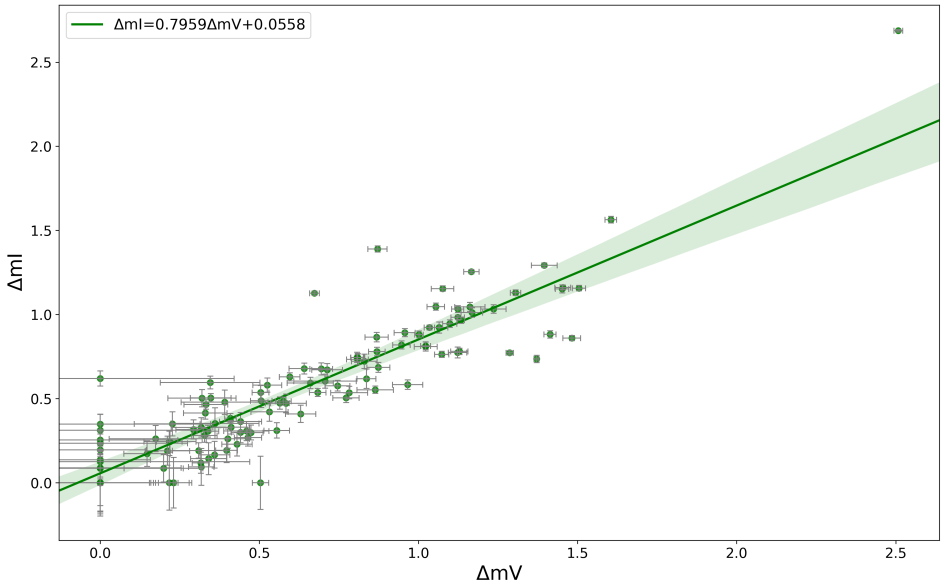


Figure 3.2: Correlation of the magnitude difference between filters Infrared and Visual. $R = 0.899$

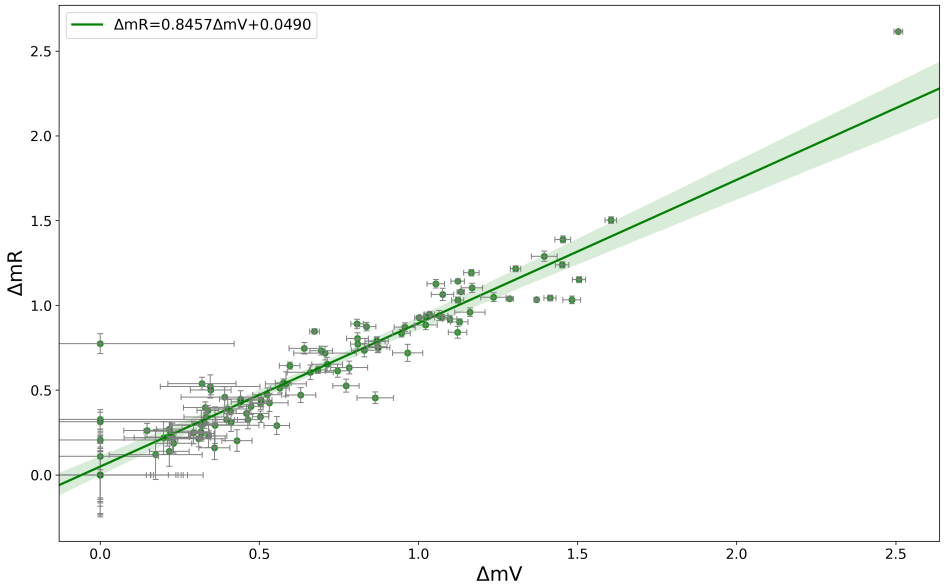


Figure 3.3: Correlation of the magnitude difference between filters Red and Visible. $R = 0.947$

## 3.2 Astrometry Results

Table 3.2 present 342 astrometric measurements of 114 star systems. The first three columns give the designation of double stars: the WDS catalog name (Worley & Douglass, 1997), filter and the official binary star discoverer designation. The fourth column gives the epoch of observation in fractions of Besselian years (2019+). The following columns contain: the separation angle $\rho$ (arcseconds) and the position angle $\theta$ (degrees) first our results and then the data from the WDS catalog of the second and more recent observation.

We present astrometric results, although is not the main objective of this thesis. Because, we obtained this without not much effort through auto correlation processing of the power spectrum. This results are so useful, if the close double stars have short time period and with some measurements, we could calculate its orbits; and if this have a long period, we can improve our calibration.

Table 3.2: Astrometry results of the April, 2019 observations.

| WDS (2000) | Filter | Discoverer designation | Epoch (2019+) | $\rho$ (arcsec) | $\theta$ (degree) | $\rho$ WDS (arcsec) | $\theta$ WDS (degree) |
|---|---|---|---|---|---|---|---|
| 20 April | | | | | | | |
| 11151+3735 | I | 5CHR 192 | 0.29955 | 0.624 | 244.41 | 0.60 | 243 |
| 11151+3735 | R | | 0.29955 | 0.652 | 244.38 | | |
| 11151+3735 | V | | 0.29954 | 0.652 | 244.33 | | |
| 13062+1621 | I | 1HEI 370 | 0.29972 | 0.996 | 287.21 | 0.90 | 287 |
| 13062+1621 | R | | 0.29972 | 0.986 | 286.96 | | |
| 13062+1621 | V | | 0.29972 | 1.001 | 286.86 | | |
| 13068+4022 | I | 2A 2062 | 0.29974 | 0.682 | 299.47 | 0.60 | 301 |
| 13068+4022 | R | | 0.29973 | 0.669 | 299.90 | | |
| 13068+4022 | V | | 0.29973 | 0.667 | 299.84 | | |
| 13134+5252 | I | 2A 1607 | 0.29980 | 0.468 | 8.36 | 0.50 | 12 |
| 13134+5252 | R | | 0.29979 | 0.468 | 8.36 | | |
| 13134+5252 | V | | 0.29979 | 0.479 | 8.83 | | |
| 13149+4055 | I | 5COU1911 | 0.29982 | 0.545 | 87.72 | 0.50 | 89 |
| 13149+4055 | R | | 0.29982 | 0.534 | 86.90 | | |
| 13149+4055 | V | | 0.29982 | 0.543 | 85.78 | | |
| 13225+4242 | I | 2COU1581 | 0.29986 | 0.345 | 156.43 | 0.30 | 158 |
| 13225+4242 | R | | 0.29985 | 0.345 | 156.41 | | |
| 13225+4242 | V | | 0.29985 | 0.354 | 156.06 | | |
| 13230+4058 | I | 8COU1582 | 0.29987 | 0.685 | 78.48 | 0.60 | 82 |

Continued on the next page.

| WDS (2000) | Filter | Discoverer designation | Epoch (2019+) | $\rho$ (arcsec) | $\theta$ (degree) | $\rho$ WDS (arcsec) | $\theta$ WDS (degree) |
|---|---|---|---|---|---|---|---|
| 13230+4058 | R | | 0.29986 | 0.670 | 78.44 | | |
| 13230+4058 | V | | 0.29986 | 0.676 | 77.85 | | |
| 16013+4529 | I | 9A 1640 | 0.30010 | 0.656 | 345.22 | 0.70 | 345 |
| 16013+4529 | R | | 0.30010 | 0.655 | 346.29 | | |
| 16013+4529 | V | | 0.30010 | 0.675 | 344.55 | | |
| 16028+4902 | I | 2HDS2264 | 0.30012 | 0.250 | 157.39 | 0.30 | 137 |
| 16028+4902 | R | | 0.30012 | 0.250 | 157.39 | | |
| 16028+4902 | V | | 0.30012 | 0.250 | 157.39 | | |
| 16043+3230 | I | 0HDS2267 | 0.30014 | 0.437 | 325.41 | 0.40 | 330 |
| 16043+3230 | R | | 0.30014 | 0.437 | 325.37 | | |
| 16043+3230 | V | | 0.30014 | 0.452 | 325.88 | | |
| 21 April | | | | | | | |
| 11247+3758 | I | 8COU1261 | 0.30221 | 0.684 | 217.37 | 0.60 | 219 |
| 11247+3758 | R | | 0.30222 | 0.685 | 217.40 | | |
| 11247+3758 | V | | 0.30222 | 0.686 | 218.13 | | |
| 11258+5527 | I | 7MLR 601 | 0.30223 | 1.060 | 55.58 | 0.70 | 55 |
| 11258+5527 | R | | 0.30223 | 1.060 | 55.58 | | |
| 11258+5527 | V | | 0.30223 | 1.061 | 55.50 | | |
| 11287+3224 | I | 4COU 781 | 0.30226 | 0.652 | 284.36 | 0.60 | 292 |
| 11287+3224 | R | | 0.30226 | 0.652 | 284.35 | | |
| 11287+3224 | V | | 0.30227 | 0.653 | 283.52 | | |
| 11297+3302 | I | 2COU 782 | 0.30228 | 0.718 | 55.30 | 0.80 | 55 |
| 11297+3302 | R | | 0.30228 | 0.718 | 55.28 | | |
| 11297+3302 | V | | 0.30228 | 0.718 | 55.28 | | |
| 11336+4729 | I | 9COU1573 | 0.30229 | 0.626 | 88.37 | 0.60 | 85 |
| 11336+4729 | R | | 0.30229 | 0.652 | 89.29 | | |
| 11336+4729 | V | | 0.30229 | 0.652 | 89.34 | | |
| 11397+5036 | I | 8COU1261 | 0.30231 | 0.468 | 64.40 | 0.50 | 66 |
| 11397+5036 | R | | 0.30231 | 0.467 | 64.39 | | |
| 11397+5036 | V | | 0.30232 | 0.470 | 66.38 | | |
| 11431+3715 | I | 5HU 1135 | 0.30233 | 0.717 | 334.46 | 0.70 | 334 |
| 11431+3715 | R | | 0.30233 | 0.717 | 334.45 | | |
| 11431+3715 | V | | 0.30233 | 0.717 | 334.47 | | |
| 11463+3131 | I | 1COU 785 | 0.30234 | 0.437 | 278.42 | 0.50 | 283 |
| 11463+3131 | R | | 0.30234 | 0.437 | 278.47 | | |

Continued on the next page.

| WDS (2000) | Filter | Discoverer designation | Epoch (2019+) | $\rho$ (arcsec) | $\theta$ (degree) | $\rho$ WDS (arcsec) | $\theta$ WDS (degree) |
|---|---|---|---|---|---|---|---|
| 11463+3131 | V | | 0.30233 | 0.437 | 278.46 | | |
| 11487+3937 | I | 7COU1263 | 0.30235 | 0.405 | 240.44 | 0.40 | 237 |
| 11487+3937 | R | | 0.30235 | 0.405 | 240.39 | | |
| 11487+3937 | V | | 0.30235 | 0.406 | 241.40 | | |
| 11487+4030 | I | 0COU1262 | 0.30234 | 0.682 | 248.50 | 0.70 | 251 |
| 11487+4030 | R | | 0.30235 | 0.683 | 248.50 | | |
| 11487+4030 | V | | 0.30235 | 0.684 | 248.46 | | |
| 11499+3754 | I | 4UR 6 | 0.30236 | 0.531 | 116.33 | 0.50 | 127 |
| 11499+3754 | R | | 0.30236 | 0.530 | 116.34 | | |
| 11499+3754 | V | | 0.30236 | 0.530 | 116.39 | | |
| 15034+3342 | I | 2TDS9384 | 0.30264 | 0.408 | 108.37 | 0.50 | 105 |
| 15034+3342 | R | | 0.30264 | 0.407 | 107.42 | | |
| 15034+3342 | V | | 0.30264 | 0.434 | 107.39 | | |
| 15062+5225 | I | 5HDS2126 | 0.30270 | 0.622 | 288.49 | 0.60 | 294 |
| 15062+5225 | R | | 0.30269 | 0.621 | 287.62 | | |
| 15062+5225 | V | | 0.30269 | 0.622 | 287.55 | | |
| 15075+5516 | I | 6UC 2929 | 0.30270 | 0.467 | 137.44 | 0.20 | 141 |
| 15075+5516 | R | | 0.30270 | 0.468 | 138.34 | | |
| 15075+5516 | V | | 0.30270 | 0.468 | 138.34 | | |
| 15088+4014 | I | 4COU1272 | 0.30271 | 0.249 | 59.41 | 0.30 | 54 |
| 15088+4014 | R | | 0.30272 | 0.249 | 59.40 | | |
| 15088+4014 | V | | 0.30272 | 0.250 | 59.38 | | |
| 15136+3453 | I | 3HO 60 | 0.30275 | 0.249 | 58.41 | 0.20 | 68 |
| 15136+3453 | R | | 0.30275 | 0.250 | 59.38 | | |
| 15136+3453 | V | | 0.30275 | 0.249 | 58.39 | | |
| 15154+3558 | I | 8HU 1273 | 0.30276 | 0.186 | 83.37 | 0.30 | 82 |
| 15154+3558 | R | | 0.30276 | 0.187 | 82.40 | | |
| 15154+3558 | V | | 0.30277 | 0.187 | 83.38 | | |
| 15192+4329 | I | 9A 1630 | 0.30283 | 0.780 | 243.36 | 0.80 | 245 |
| 15192+4329 | R | | 0.30283 | 0.780 | 243.32 | | |
| 15192+4329 | V | | 0.30283 | 0.779 | 242.46 | | |
| 15200+4603 | I | 3A 1631 | 0.30284 | 0.748 | 251.42 | 0.80 | 260 |
| 15200+4603 | R | | 0.30284 | 0.748 | 251.35 | | |
| 15200+4603 | V | | 0.30284 | 0.747 | 249.66 | | |

22 April

Continued on the next page.

| WDS (2000) | Filter | Discoverer designation | Epoch (2019+) | $\rho$ (arcsec) | $\theta$ (degree) | $\rho$ WDS (arcsec) | $\theta$ WDS (degree) |
|---|---|---|---|---|---|---|---|
| 18062+3326 | I | 6HO 79 | 0.30537 | 0.248 | 48.39 | 0.20 | 39 |
| 18062+3326 | R | | 0.30537 | 0.219 | 49.38 | | |
| 18062+3326 | V | | 0.30537 | 0.248 | 46.41 | | |
| 14040+4314 | I | 4A 1615 | 0.30487 | 0.527 | 0.44 | 0.60 | 4 |
| 14040+4314 | R | | 0.30487 | 0.501 | 0.46 | | |
| 14040+4314 | V | | 0.30487 | 0.501 | 0.34 | | |
| 14048+3243 | I | 3COU 603 | 0.30487 | 0.687 | 55.35 | 0.70 | 53 |
| 14048+3243 | R | | 0.30488 | 0.688 | 55.28 | | |
| 14048+3243 | V | | 0.30488 | 0.688 | 56.09 | | |
| 14059+3848 | I | 8HU 1263 | 0.30489 | 0.284 | 17.37 | 0.30 | 20 |
| 14059+3848 | R | | 0.30488 | 0.283 | 16.38 | | |
| 14059+3848 | V | | 0.30488 | 0.284 | 12.47 | | |
| 14059+4059 | I | 9COU1585 | 0.30489 | 0.906 | 214.77 | 0.90 | 214 |
| 14059+4059 | R | | 0.30489 | 0.905 | 214.64 | | |
| 14059+4059 | V | | 0.30489 | 0.906 | 214.63 | | |
| 14122+4411 | I | 1STT 278 | 0.30492 | 0.376 | 269.41 | 0.40 | 273 |
| 14122+4411 | R | | 0.30492 | 0.376 | 269.40 | | |
| 14122+4411 | V | | 0.30491 | 0.376 | 269.39 | | |
| 14171+4529 | I | 9A 1617 | 0.30496 | 0.467 | 282.34 | 0.40 | 280 |
| 14171+4529 | R | | 0.30496 | 0.467 | 282.34 | | |
| 14171+4529 | V | | 0.30496 | 0.467 | 281.43 | | |
| 14171+5100 | I | 0A 147 | 0.30497 | 0.593 | 106.42 | 0.70 | 109 |
| 14171+5100 | R | | 0.30497 | 0.593 | 106.39 | | |
| 14171+5100 | V | | 0.30498 | 0.593 | 106.38 | | |
| 14184+3412 | I | 2HU 901 | 0.30499 | 0.622 | 36.37 | 0.60 | 36 |
| 14184+3412 | R | | 0.30498 | 0.622 | 36.39 | | |
| 14184+3412 | V | | 0.30498 | 0.622 | 36.35 | | |
| 14188+5934 | I | 4HU 1267 | 0.30499 | 0.747 | 185.22 | 0.50 | 178 |
| 14188+5934 | R | | 0.30500 | 0.747 | 185.32 | | |
| 14188+5934 | V | | 0.30500 | 0.775 | 185.37 | | |
| 14220+5107 | I | 7A 148 | 0.30503 | 0.496 | 189.40 | 0.50 | 192 |
| 14220+5107 | R | | 0.30503 | 0.497 | 189.39 | | |
| 14220+5107 | V | | 0.30502 | 0.497 | 189.39 | | |
| 14289+4226 | I | 6COU1758 | 0.30529 | 0.592 | 148.20 | 0.60 | 147 |
| 14289+4226 | R | | 0.30529 | 0.592 | 147.40 | | |

Continued on the next page.

| WDS (2000) | Filter | Discoverer designation | Epoch (2019+) | $\rho$ (arcsec) | $\theta$ (degree) | $\rho$ WDS (arcsec) | $\theta$ WDS (degree) |
|---|---|---|---|---|---|---|---|
| 14289+4226 | V | | 0.30529 | 0.562 | 150.24 | | |
| 18017+4011 | I | 1STF2267 | 0.30531 | 0.499 | 277.40 | 0.40 | 281 |
| 18017+4011 | R | | 0.30530 | 0.499 | 277.40 | | |
| 18017+4011 | V | | 0.30530 | 0.500 | 277.39 | | |
| 18036+3731 | I | 1COU1147 | 0.30531 | 0.717 | 178.38 | 0.70 | 175 |
| 18036+3731 | R | | 0.30531 | 0.717 | 177.63 | | |
| 18036+3731 | V | | 0.30532 | 0.718 | 177.57 | | |
| 18054+4306 | I | 6COU1787 | 0.30534 | 0.375 | 322.47 | 0.50 | 323 |
| 18054+4306 | R | | 0.30534 | 0.375 | 322.39 | | |
| 18054+4306 | V | | 0.30534 | 0.375 | 322.41 | | |
| 18054+5155 | I | 5COU2513 | 0.30535 | 0.903 | 56.23 | 0.80 | 54 |
| 18054+5155 | R | | 0.30535 | 0.904 | 56.29 | | |
| 18054+5155 | V | | 0.30535 | 0.903 | 56.31 | | |
| 18063+3824 | I | 4HU 1186 | 0.30538 | 0.126 | 143.39 | 0.40 | 125 |
| 18063+3824 | R | | 0.30538 | 0.127 | 144.40 | | |
| 18063+3824 | V | | 0.30538 | 0.126 | 144.39 | | |
| 18064+4437 | I | 7COU1926 | 0.30539 | 0.310 | 122.37 | 0.30 | 124 |
| 18064+4437 | R | | 0.30539 | 0.310 | 122.36 | | |
| 18064+4437 | V | | 0.30539 | 0.313 | 122.36 | | |
| 10056+3105 | I | 5STF1406 | 0.30546 | 0.749 | 216.47 | 0.70 | 219 |
| 10056+3105 | R | | 0.30547 | 0.749 | 216.46 | | |
| 10056+3105 | V | | 0.30547 | 0.749 | 216.42 | | |
| 10059+5731 | I | 1TDS7012 | 0.30548 | 0.592 | 101.54 | 0.60 | 102 |
| 10059+5731 | R | | 0.30548 | 0.592 | 101.51 | | |
| 10059+5731 | V | | 0.30547 | 0.592 | 101.46 | | |
| 10095+4126 | I | 6A 2143 | 0.30568 | 0.281 | 162.40 | 0.50 | 126 |
| 10095+4126 | R | | 0.30568 | 0.282 | 162.39 | | |
| 10095+4126 | V | | 0.30569 | 0.282 | 162.41 | | |
| 10118+4222 | I | 2POP 116 | 0.30570 | 0.531 | 250.36 | 0.50 | 248 |
| 10118+4222 | R | | 0.30570 | 0.531 | 249.43 | | |
| 10118+4222 | V | | 0.30570 | 0.530 | 249.47 | | |
| 10164+4003 | I | 3A 2147 | 0.30572 | 0.966 | 276.38 | 0.90 | 277 |
| 10164+4003 | R | | 0.30572 | 0.967 | 276.39 | | |
| 10164+4003 | V | | 0.30572 | 0.995 | 276.44 | | |
| 10261+5347 | I | 7MLR 679 | 0.30576 | 1.092 | 262.32 | 1.10 | 263 |

Continued on the next page.

| WDS (2000) | Filter | Discoverer designation | Epoch (2019+) | $\rho$ (arcsec) | $\theta$ (degree) | $\rho$ WDS (arcsec) | $\theta$ WDS (degree) |
|---|---|---|---|---|---|---|---|
| 10261+5347 | R | | 0.30576 | 1.120 | 263.16 | | |
| 10261+5347 | V | | 0.30576 | 1.120 | 262.53 | | |
| 23 April | | | | | | | |
| 12056+5659 | I | 9YSC 211 | 0.30773 | 0.529 | 48.46 | 0.50 | 50 |
| 12056+5659 | R | | 0.30774 | 0.529 | 48.42 | | |
| 12056+5659 | V | | 0.30775 | 0.529 | 49.38 | | |
| 12080+4242 | I | 2A 1998 | 0.30786 | 0.283 | 344.38 | 0.30 | 345 |
| 12080+4242 | R | | 0.30786 | 0.283 | 344.39 | | |
| 12080+4242 | V | | 0.30787 | 0.309 | 343.34 | | |
| 12092+5013 | I | 3COU2102 | 0.30788 | 0.406 | 303.45 | 0.40 | 293 |
| 12092+5013 | R | | 0.30787 | 0.406 | 303.37 | | |
| 12092+5013 | V | | 0.30787 | 0.404 | 303.48 | | |
| 12160+4807 | I | 7HU 736 | 0.30792 | 0.375 | 178.43 | 0.30 | 189 |
| 12160+4807 | R | | 0.30792 | 0.375 | 179.35 | | |
| 12160+4807 | V | | 0.30792 | 0.374 | 179.39 | | |
| 12195+4456 | I | 6COU1753 | 0.30792 | 0.655 | 119.51 | 0.90 | 110 |
| 12195+4456 | R | | 0.30793 | 0.655 | 119.48 | | |
| 12195+4456 | V | | 0.30793 | 0.655 | 119.48 | | |
| 12215+5014 | I | 4HDS1741 | 0.30794 | 0.225 | 28.38 | 0.20 | 22 |
| 12215+5014 | R | | 0.30794 | 0.223 | 29.37 | | |
| 12215+5014 | V | | 0.30793 | 0.225 | 29.39 | | |
| 16026+4658 | I | 8COU1765 | 0.30813 | 0.810 | 99.76 | 0.60 | 100 |
| 16026+4658 | R | | 0.30814 | 0.811 | 100.52 | | |
| 16026+4658 | V | | 0.30814 | 0.837 | 99.58 | | |
| 16028+4902 | I | 2HDS2264 | 0.30815 | 0.250 | 157.36 | 0.30 | 137 |
| 16028+4902 | R | | 0.30814 | 0.250 | 157.39 | | |
| 16028+4902 | V | | 0.30814 | 0.252 | 161.34 | | |
| 16061+5652 | I | 2TDS 802 | 0.30821 | 0.841 | 308.44 | 0.80 | 302 |
| 16061+5652 | R | | 0.30821 | 0.841 | 308.46 | | |
| 16061+5652 | V | | 0.30821 | 0.840 | 306.86 | | |
| 16097+4900 | I | 0COU1919 | 0.30824 | 0.747 | 132.51 | 0.50 | 141 |
| 16097+4900 | R | | 0.30824 | 0.747 | 132.46 | | |
| 16097+4900 | V | | 0.30824 | 0.748 | 132.48 | | |
| 16107+4019 | I | 9COU1277 | 0.30825 | 0.685 | 349.26 | 0.90 | 350 |
| 16107+4019 | R | | 0.30825 | 0.685 | 348.49 | | |

Continued on the next page.

| WDS (2000) | Filter | Discoverer designation | Epoch (2019+) | $\rho$ (arcsec) | $\theta$ (degree) | $\rho$ WDS (arcsec) | $\theta$ WDS (degree) |
|---|---|---|---|---|---|---|---|
| 16107+4019 | V | | 0.30824 | 0.685 | 348.56 | | |
| 16128+3922 | I | 2STF2028 | 0.30827 | 0.500 | 146.37 | 0.40 | 144 |
| 16128+3922 | R | | 0.30827 | 0.500 | 146.37 | | |
| 16128+3922 | V | | 0.30827 | 0.500 | 146.38 | | |
| 16137+4638 | I | 8A 1642 | 0.30828 | 0.842 | 179.27 | 0.80 | 181 |
| 16137+4638 | R | | 0.30828 | 0.842 | 179.31 | | |
| 16137+4638 | V | | 0.30828 | 0.842 | 179.34 | | |
| 16140+4200 | I | 0COU1449 | 0.30828 | 0.156 | 114.40 | 0.30 | 161 |
| 16140+4200 | R | | 0.30829 | 0.155 | 114.39 | | |
| 16140+4200 | V | | 0.30829 | 0.155 | 114.39 | | |
| 16172+3341 | I | 1COU 980 | 0.30829 | 0.530 | 335.35 | 0.50 | 343 |
| 16172+3341 | R | | 0.30829 | 0.530 | 335.41 | | |
| 16172+3341 | V | | 0.30829 | 0.531 | 334.52 | | |
| 16173+5001 | I | 1COU2111 | 0.30830 | 0.314 | 30.36 | 0.30 | 33 |
| 16173+5001 | R | | 0.30830 | 0.314 | 29.40 | | |
| 16173+5001 | V | | 0.30830 | 0.314 | 31.38 | | |
| 16178+4918 | I | 8HU 661 | 0.30831 | 0.776 | 40.28 | 0.90 | 38 |
| 16178+4918 | R | | 0.30830 | 0.777 | 40.31 | | |
| 16178+4918 | V | | 0.30830 | 0.777 | 40.30 | | |
| 16192+4140 | I | 0STT 309 | 0.30832 | 0.281 | 317.36 | 0.30 | 310 |
| 16192+4140 | R | | 0.30832 | 0.281 | 317.38 | | |
| 16192+4140 | V | | 0.30832 | 0.281 | 317.38 | | |
| 16216+3631 | I | 1COU 982 | 0.30833 | 0.406 | 250.44 | 0.30 | 230 |
| 16216+3631 | R | | 0.30833 | 0.407 | 250.43 | | |
| 16216+3631 | V | | 0.30833 | 0.407 | 250.43 | | |
| 24 April | | | | | | | |
| 10477+2733 | I | 3COU 592 | 0.31051 | 0.436 | 30.39 | 0.40 | 29 |
| 10477+2733 | R | | 0.31051 | 0.437 | 32.31 | | |
| 10477+2733 | V | | 0.31051 | 0.436 | 30.41 | | |
| 10486+3532 | I | 2COU1418 | 0.31050 | 0.777 | 209.41 | 0.80 | 209 |
| 10486+3532 | R | | 0.31050 | 0.778 | 209.45 | | |
| 10486+3532 | V | | 0.31050 | 0.779 | 210.29 | | |
| 10529+2209 | I | 9HU 567 | 0.31042 | 0.437 | 197.35 | 0.50 | 197 |
| 10529+2209 | R | | 0.31043 | 0.438 | 196.45 | | |
| 10529+2209 | V | | 0.31043 | 0.438 | 196.43 | | |

Continued on the next page.

| WDS (2000) | Filter | Discoverer designation | Epoch (2019+) | $\rho$ (arcsec) | $\theta$ (degree) | $\rho$ WDS (arcsec) | $\theta$ WDS (degree) |
|---|---|---|---|---|---|---|---|
| 10543+2607 | I | 7A 1769 | 0.31041 | 0.745 | 83.55 | 0.70 | 82 |
| 10543+2607 | R | | 0.31041 | 0.745 | 83.51 | | |
| 10543+2607 | V | | 0.31041 | 0.745 | 83.49 | | |
| 10544+2044 | I | 4HU 568 | 0.31039 | 0.746 | 354.50 | 0.70 | 353 |
| 10544+2044 | R | | 0.31039 | 0.747 | 354.46 | | |
| 10544+2044 | V | | 0.31039 | 0.747 | 354.45 | | |
| 10544+3840 | I | 0COU1746 | 0.31036 | 0.313 | 332.36 | 0.30 | 331 |
| 10544+3840 | R | | 0.31036 | 0.313 | 332.38 | | |
| 10544+3840 | V | | 0.31036 | 0.312 | 333.34 | | |
| 10548+2345 | I | 5BU 597 | 0.31035 | 1.026 | 44.46 | 0.90 | 47 |
| 10548+2345 | R | | 0.31035 | 1.027 | 44.44 | | |
| 10548+2345 | V | | 0.31035 | 1.027 | 44.42 | | |
| 10567+3320 | I | 0POP 73 | 0.31030 | 0.778 | 200.44 | 0.70 | 202 |
| 10567+3320 | R | | 0.31031 | 0.778 | 200.47 | | |
| 10567+3320 | V | | 0.31031 | 0.778 | 200.46 | | |
| 10574+0147 | I | 7HEI 763 | 0.31034 | 0.810 | 252.28 | 0.80 | 251 |
| 10574+0147 | R | | 0.31034 | 0.811 | 251.48 | | |
| 10574+0147 | V | | 0.31033 | 0.811 | 251.48 | | |
| 10585+1711 | I | 1A 2375 | 0.31032 | 0.531 | 167.44 | 0.50 | 169 |
| 10585+1711 | R | | 0.31033 | 0.531 | 167.44 | | |
| 10585+1711 | V | | 0.31033 | 0.531 | 167.41 | | |
| 14317+3554 | I | 4COU1267 | 0.30817 | 0.745 | 60.66 | 0.90 | 85 |
| 14317+3554 | R | | 0.31091 | 0.745 | 60.66 | | |
| 14317+3554 | V | | 0.31091 | 0.745 | 60.66 | | |
| 14340+4500 | I | 0COU1587 | 0.31090 | 0.778 | 26.21 | 0.80 | 27 |
| 14340+4500 | R | | 0.31090 | 0.778 | 25.38 | | |
| 14340+4500 | V | | 0.31090 | 0.778 | 26.26 | | |
| 14460+4723 | I | 3HDS2079 | 0.31082 | 0.715 | 313.32 | 0.70 | 314 |
| 14460+4723 | R | | 0.31082 | 0.716 | 313.33 | | |
| 14460+4723 | V | | 0.31082 | 0.716 | 313.41 | | |
| 14487+4513 | I | 3TDS9314 | 0.31081 | 0.748 | 274.31 | 0.70 | 274 |
| 14487+4513 | R | | 0.31081 | 0.748 | 274.33 | | |
| 14487+4513 | V | | 0.31081 | 0.773 | 274.45 | | |
| 14492+4814 | I | 4HU 647 | 0.31081 | 0.157 | 75.39 | 0.30 | 69 |
| 14492+4814 | R | | 0.31080 | 0.158 | 75.39 | | |

Continued on the next page.

| WDS (2000) | Filter | Discoverer designation | Epoch (2019+) | $\rho$ (arcsec) | $\theta$ (degree) | $\rho$ WDS (arcsec) | $\theta$ WDS (degree) |
|---|---|---|---|---|---|---|---|
| 14492+4814 | V | | 0.31080 | 0.158 | 74.40 | | |
| 14515+4456 | I | 6STT 287 | 0.31080 | 0.562 | 5.39 | 0.60 | 5 |
| 14515+4456 | R | | 0.31080 | 0.561 | 5.38 | | |
| 14515+4456 | V | | 0.31080 | 0.562 | 5.38 | | |
| 14558+3939 | I | 9A 1627 | 0.31078 | 0.220 | 205.40 | 0.20 | 183 |
| 14558+3939 | R | | 0.31078 | 0.220 | 205.39 | | |
| 14558+3939 | V | | 0.31078 | 0.220 | 205.40 | | |
| 14571+5136 | I | 6TDS9350 | 0.31077 | 0.933 | 122.58 | 0.90 | 123 |
| 14571+5136 | R | | 0.31077 | 0.932 | 122.46 | | |
| 14571+5136 | V | | 0.31077 | 0.907 | 123.24 | | |
| 14575+3124 | I | 4HDS2112 | 0.31076 | 0.748 | 339.47 | 0.80 | 335 |
| 14575+3124 | R | | 0.31075 | 0.749 | 339.44 | | |
| 14575+3124 | V | | 0.31075 | 0.749 | 339.44 | | |
| 14593+4649 | I | 9COU1760 | 0.31074 | 0.160 | 267.39 | 0.20 | 249 |
| 14593+4649 | R | | 0.31074 | 0.184 | 266.40 | | |
| 14593+4649 | V | | 0.31075 | 0.185 | 265.40 | | |
| 16013+4529 | I | 9A 1640 | 0.31094 | 0.655 | 345.26 | 0.70 | 345 |
| 16013+4529 | R | | 0.31095 | 0.656 | 344.47 | | |
| 16013+4529 | V | | 0.31095 | 0.655 | 345.24 | | |
| 16026+4658 | I | 8COU1765 | 0.31097 | 0.810 | 100.48 | 0.60 | 100 |
| 16026+4658 | R | | 0.31095 | 0.810 | 100.43 | | |
| 16026+4658 | V | | 0.31095 | 0.811 | 100.52 | | |
| 16028+4902 | I | 2HDS2264 | 0.31096 | 0.250 | 156.41 | 0.30 | 137 |
| 16028+4902 | R | | 0.31096 | 0.250 | 157.38 | | |
| 16028+4902 | V | | 0.31096 | 0.250 | 157.38 | | |
| 16107+4019 | I | 9COU1277 | 0.31104 | 0.684 | 349.26 | 0.90 | 350 |
| 16107+4019 | R | | 0.31103 | 0.685 | 348.48 | | |
| 16107+4019 | V | | 0.31103 | 0.684 | 349.28 | | |
| 16118+3424 | I | 4STT 306 | 0.31104 | 0.217 | 359.40 | 0.20 | 11 |
| 16118+3424 | R | | 0.31104 | 0.218 | 0.38 | | |
| 16118+3424 | V | | 0.31104 | 0.218 | 0.39 | | |
| 25 April | | | | | | | |
| 09043+4008 | I | 8COU2498 | 0.31303 | 0.812 | 244.50 | 0.80 | 244 |
| 09043+4008 | R | | 0.31302 | 0.812 | 244.44 | | |
| 09043+4008 | V | | 0.31302 | 0.812 | 244.42 | | |

Continued on the next page.

| WDS (2000) | Filter | Discoverer designation | Epoch (2019+) | $\rho$ (arcsec) | $\theta$ (degree) | $\rho$ WDS (arcsec) | $\theta$ WDS (degree) |
|---|---|---|---|---|---|---|---|
| 09067+5038 | I | 8HU 722 | 0.31305 | 0.497 | 237.36 | 0.50 | 244 |
| 09067+5038 | R | | 0.31305 | 0.498 | 237.37 | | |
| 09067+5038 | V | | 0.31305 | 0.498 | 237.36 | | |
| 09100+4034 | I | 4COU2499 | 0.31307 | 0.593 | 36.43 | 0.60 | 37 |
| 09100+4034 | R | | 0.31307 | 0.593 | 36.35 | | |
| 09100+4034 | V | | 0.31307 | 0.593 | 36.36 | | |
| 09171+4040 | I | 0A 1981 | 0.31310 | 0.252 | 339.42 | 0.30 | 339 |
| 09171+4040 | R | | 0.31310 | 0.252 | 339.42 | | |
| 09171+4040 | V | | 0.31309 | 0.252 | 339.42 | | |
| 09172+4038 | I | 8A 1982 | 0.31311 | 0.280 | 339.39 | 0.20 | 315 |
| 09172+4038 | R | | 0.31311 | 0.281 | 339.39 | | |
| 09172+4038 | V | | 0.31311 | 0.281 | 340.38 | | |
| 09224+4616 | I | 6A 1758 | 0.31313 | 0.590 | 308.30 | 0.50 | 308 |
| 09224+4616 | R | | 0.31313 | 0.590 | 308.30 | | |
| 09224+4616 | V | | 0.31313 | 0.590 | 308.30 | | |
| 13033+3435 | I | 5COU 970 | 0.31340 | 0.249 | 102.38 | 0.20 | 94 |
| 13033+3435 | R | | 0.31340 | 0.250 | 102.38 | | |
| 13033+3435 | V | | 0.31340 | 0.249 | 103.38 | | |
| 13068+4022 | I | 2A 2062 | 0.31345 | 0.657 | 300.28 | 0.60 | 301 |
| 13068+4022 | R | | 0.31345 | 0.683 | 299.50 | | |
| 13068+4022 | V | | 0.31345 | 0.684 | 299.52 | | |
| 13120+4703 | I | 3COU2106 | 0.31347 | 0.190 | 89.40 | 0.30 | 91 |
| 13120+4703 | R | | 0.31348 | 0.190 | 89.40 | | |
| 13120+4703 | V | | 0.31348 | 0.189 | 89.41 | | |
| 13134+5252 | I | 2A 1607 | 0.31349 | 0.468 | 8.38 | 0.50 | 12 |
| 13134+5252 | R | | 0.31349 | 0.468 | 8.39 | | |
| 13134+5252 | V | | 0.31348 | 0.468 | 9.35 | | |
| 13149+4055 | I | 5COU1911 | 0.31350 | 0.531 | 87.29 | 0.50 | 89 |
| 13149+4055 | R | | 0.31350 | 0.531 | 87.28 | | |
| 13149+4055 | V | | 0.31350 | 0.530 | 87.32 | | |
| 17007+3951 | I | 1COU1290 | 0.31374 | 0.714 | 28.35 | 0.70 | 27 |
| 17007+3951 | R | | 0.31374 | 0.714 | 28.36 | | |
| 17007+3951 | V | | 0.31374 | 0.714 | 28.35 | | |
| 17043+4445 | I | 5COU1593 | 0.31378 | 0.497 | 198.32 | 0.60 | 191 |
| 17043+4445 | R | | 0.31378 | 0.498 | 198.32 | | |

Continued on the next page.

| WDS (2000) | Filter | Discoverer designation | Epoch (2019+) | $\rho$ (arcsec) | $\theta$ (degree) | $\rho$ WDS (arcsec) | $\theta$ WDS (degree) |
|---|---|---|---|---|---|---|---|
| 17043+4445 | V | | 0.31377 | 0.498 | 198.32 | | |
| 17073+4604 | I | 4COU1773 | 0.31379 | 0.933 | 22.56 | 0.90 | 22 |
| 17073+4604 | R | | 0.31379 | 0.933 | 22.55 | | |
| 17073+4604 | V | | 0.31379 | 0.934 | 22.60 | | |
| 17075+5126 | I | 6COU1921 | 0.31381 | 0.528 | 287.34 | 0.50 | 285 |
| 17075+5126 | R | | 0.31381 | 0.527 | 285.45 | | |
| 17075+5126 | V | | 0.31381 | 0.528 | 287.33 | | |
| 17076+4108 | I | 8COU1292 | 0.31382 | 0.526 | 164.43 | 0.50 | 164 |
| 17076+4108 | R | | 0.31382 | 0.501 | 164.52 | | |
| 17076+4108 | V | | 0.31382 | 0.500 | 164.46 | | |
| 17088+4856 | I | 6COU1774 | 0.31383 | 0.593 | 97.47 | 0.40 | 105 |
| 17088+4856 | R | | 0.31383 | 0.593 | 97.44 | | |
| 17088+4856 | V | | 0.31383 | 0.593 | 97.46 | | |

# 4

# Conclusions

We present results of differential photometry in three filters VRI for 114 close binary stars. We were able to calculate magnitude differences for them. In total 342 photometric measurements are reported here. The separations of these stars ranges for $0.''2$ and $1''$ and magnitudes of the primary stars are between 8 and 11. We chose these stars because they can be measured only by using a high resolution method. The observations of these stars were performed in April of 2019 at the Observatorio Astronómico Nacional (OAN) in the Sierra of San Pedro Mártir with the Speckle Interferometer (Figure 2.2), which has high sensitive EMCCD camera iXon Ultra 888 from Andor Technology.

We improved the calculation of magnitude differences of (Pluzhnik, 2005). We found that the results are more stable, graphing $\alpha_\nu$ on the Y axis and $\beta_\nu$ on the X, and fitting the slope by the method of least squares, to obtain $C(\nu)$, as can be seen in Figure 2.8. This was done instead of fitting the quotient $C(\nu) = \frac{2\alpha_\nu}{\beta_\nu}$, directly.

Mainly, we calculated the correlation between filters. The value of the slope of equations 3.1 and 3.2 shows that the magnitude differences are larger for the red filter than for the blue one. However, this is a very preliminary result and we need more points to better determine the slopes. The scatter diagrams (Figures 3.1, 3.2 and 3.3) show the correlation between the magnitude difference measured with the different filters. These results show clearly, the linear correlation between any pair of filters; this is something to be expected given that, in general, the secondary stars are of late type.

Also, we present the astrometric parameters of the binary systems; although this was not the main objective of this thesis. We obtained the astrometric parameters with little effort, through the auto correlation processing of the power spectrum. Also we compare

our parameters with the astrometric parameters of WDS catalogue (Worley & Douglass, 1997) of the second and more recent observation.

Finally, we obtained the transformation coefficients for differential photometry (see the appendix) for filters V and R. This is a preliminary result because we do not have observations of standard stars to do a best fit, although we present an example of the procedure. This assignment is more to describe the instrument and is not the main objective of this thesis. However, this analysis is necessary to present the results in a standard system.

The results of this research will be published in Revista Mexicana de Astronomía y Astrofísica (RevMexAA) with the title: VRI Differential Photometry of Close Double Stars at Telescopes OAN. First results.

# 5

# Appendix

## 5.1 Transformation coefficients for differential photometry

Based on Benson (1998) the true apparent V magnitude of a star, assuming the atmospheric effect is not dependent on the color of the star, is then:

$$V = v + k_v * X + T_v * (V - R) + C, \tag{5.1}$$

where V is the true apparent apparent magnitude, v is the instrumental V magnitude, $k_v$ is the atmospheric extinction coefficient, X is the airmass, (V-R) is the true color index of the star, $T_{vr}$ is a transform coefficient for the V-R color, and C is a constant which may vary from night to night and depends on the efficiency of the telescope, filter, CCD combination and the zero magnitude scale used.

Our observations were performed on the filters VRI, but we do not have observations of standard stars for each filter. However, we present a example to determine the instrumental coefficient transformation of V and R filters for a fourty one stars, through the instrumental values of v and r (total photonic fluxe of double systems) and magnitudes obtained from SIMBAD Astronomical Database. We did not obtain the transformation coefficient for filter I, because the magnitude to our systems are not reported in SIMBAD for this filter.

With the assumption there is a linear relation between the standard colors and the instrumental colors. First, we plot on the X-axis V-R and in Y- axis V-v or R-r, then do a least square linear fit yielding the following equation:

$$V - v = slope * (V - R) + intercept, \tag{5.2}$$

where $intercept = k_v * X + C$ and the transformation coefficient $T_v$ is obtained from the

slope of the fit. The expressions to obtain the magnitudes $V_c$ and $R_c$ with the transformations coefficients obtained from their respective square linear fit (see Figures 5.1 and 5.2) are given by:

$$V_c = v + (7.2225 \pm 5.5530) - (1.5797 \mp 1.2623) * (V - R), \tag{5.3}$$

$$R_c = r + (5.2208 \pm 3.6439) - (1.4672 \mp 0.8283) * (V - R). \tag{5.4}$$

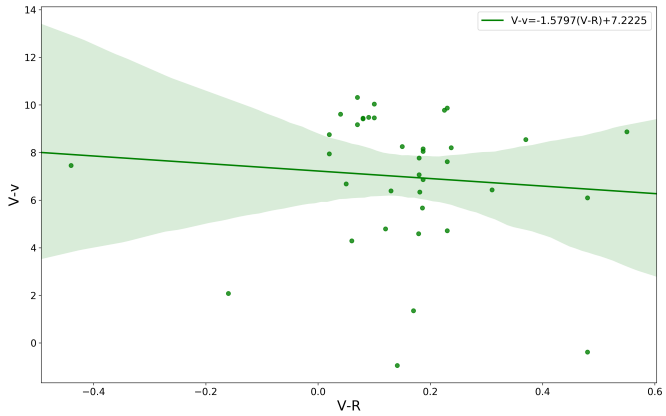


Figure 5.1: Least square linear fit yielding to obtain the transformation coefficient to V filter.

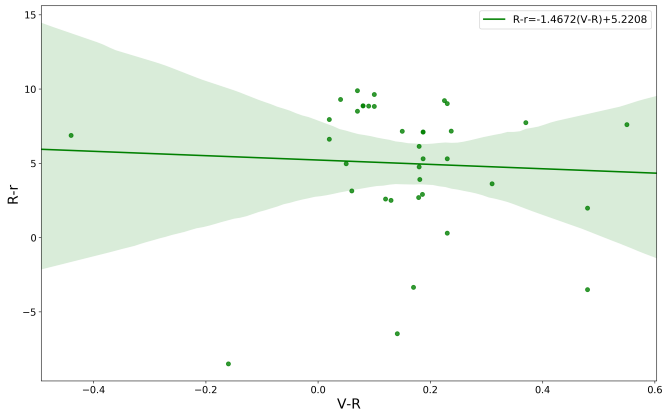


Figure 5.2: Least square linear fit yielding to obtain the transformation coefficient to R filter.

# Bibliography


Baldwin, J. E., Beckett, M. G., Boysen, R. C., et al., 1996, A&A, 306, L13-L16

Balega, I. I., Balega, Y. Y., Maksimov, A. F., et al., 1999, A&AS, 140, 287

Balega, I. I., Balega, Y. Y., Hofmann, K. H., et al., 2002, A&A, 385, 87

Balega, I. I., Balega, Y. Y., Maksimov1, A. F., Pluzhnik, E. A., Schertl, D., Shkhagosheva, Z. U., & Weigelt, G., 2004, A&A, 422, 627

Beavers, W., Dudgeon, D., & Beletic, J., 1989, Lincoln Laboratory Journal.

Benson, P. J., 1998, Whitin Observatory, Welley College, I.A.P.P. Comunications No. 72, 42-52

Christou, J. C., Ribak, E., Hege, E. K., & Freeman, J. D., 1986, Optical Engineering, 25, 724

Dainty, J. C., & A. H. Greenaway, 1979, J. Opt. Soc. Am., 69, 786

Dommanget, J., & Lampens, P., 1993, Astrophys Space Sci, 200, 221-238

Docobo, J. A., V. S. Tamazian, Yu. Yu. Balega, J. Blanco, A. F. Maximov, & V. A. Vasyuk, 2001, *A&A*, 366, 868

ESA 1997, The Hipparcos and Tycho Catalogues (ESA SP-1200; Noordwijk: European Space Agency)

Fabricius, C., Høg, E., Makarov, V. V., Mason, B. D., Wycoff, G. L., & Urban, S. E., 2002, *A&A*, 384, 180

Guerrero, C. A., Orlov, V. G., Borges Fernandes, M., & Ángeles, F., 2018, MNRAS 475, 1725

Hartkopf, W. I., McAlister, H. A., & Mason, B. D. 2001, AJ, 122, 3480. Electronic version: https://www.usno.navy.mil/USNO/astrometry/optical-IR-prod/wds/int4

Hartkopf, W.I., & Mason, B.D., 2011, AJ 142, 56

Karttunen, H.,Kroger, P., Oja, H., Poutanen, M., & Donner, K. J. (2007). Fundamental Astronomy. Berlin Heidelberg New York: Springer

Kerp, J., Barth, W., Hofmann, K., Reinheimer, T., & Weigelt, G. in , ESO Conference on High-Resolution Imaging by Interferometry II, ed. J. BeckersF. Merkle, 1992, 1, 269278

Kohler, R., 204 ASP Conference Series, 318

Labeyrie, A., 1970, A&A, 6, 85

Lena, P., 1987, The Messenger, 50, 53

Mason B. D., et al., 2017, AJ, 153, 20

McAlister, H. A., Bagnuolo, W. G., Hartkopf, W.I., et al., 1990, Proc. SPIE, 22

Men'shchikov A. B., Balega Y. Y., Berger M., Driebe T., Hofmann K. H., Maximov A. F., Schert D., Shenavrin V. I., & Weigelt G., 2006, A & A, 448, 271-281

Miles, S. K. N., & Mason, B. D., 2017, Inf. Circ. 191, 1

Ling, J. F.,2012, AJ, 143, 20

Orlov, V. G., Voitsekhovich, V. V., Mendoza-Valencia, G. A., Svyryd, A., Rivera, J. L., Ortiz, F., & Guerrero, C. A., 2009, Rev. Mex. Astron. Astros., 45, 155-159

Orlov V. G., Voitsekhovich V. V., 2015, Rev. Mex. Astron. Astros., 51, 67

Pluzhnik E. A., 2005, A&A, 431, 587

Prieur, J. L., Scardia, M., Pansecchi, L., Argyle, R. W., Zanutta, A., & Aristidi, E., 2016, Astronomische Nachrichten, 338, Issue 1, 74-90

Roddier, F., 1986, Opt. Commun. 60, 145-148.

Soderhjelm, S., 1999, A&A 341, 121

Tokovinin, A., & Cantarutti, R., 2008, PASP, 120, pp. 170-177

Tokovinin, A., Mason, B. D., Hartkopf, W. I., et al. 2015, AJ, 150, 50 (SOAR14)

Tokovinin, A., Mason, B. D., Hartkopf, W. I., et al. 2016b, AJ, 152, 116 van Leeuwen, F. 2007, A&A, 474, 653

Worley, C. E., & Douglass, G. G. 1997, A&AS, 125, 523. Electronic version: http://www.usno.navy.mil/USNO/astrometry/optical-IR-prod/wds/WDS